# Optical Exciton-Magnon Absorption in $MnF_2$*

D. D. SELL,† R. L. GREENE, AND ROBERT M. WHITE‡
*Department of Physics, Stanford University, Stanford, California*
(Received 22 December 1966)

We present the results of a detailed theoretical and experimental investigation of the ${}^6A_{1g}$ to ${}^4T_{1g}$ optical absorption in $MnF_2$. This transition is one in which a spin-wave sideband was identified in an earlier communication. A collective-mode theory of the excitations associated with the $Mn^{2+}$ ions is developed. Excitations within the orbital ground-electronic state correspond to the familiar spin waves, while excitations involving the excited electronic states correspond to Frenkel excitons. The symmetry of these excitations is determined and is employed to develop the selection rules for optical absorption. It is shown that the two magnetic dipole absorptions in $\sigma$ polarization (denoted $E1$ and $E2$) correspond to the excitation of $\mathbf{k}=0$ excitons. It is also shown that the three sideband absorptions (denoted $\pi 1$, $\sigma 1$, and $\sigma 2$) correspond to processes in which an exciton with a wave vector in the vicinity of the Brillouin zone is generated simultaneously with a spin wave of opposite wave vector. The theoretical position, shape, temperature dependence, and magnetic field dependence of these sidebands is shown to agree well with observation. The application of the theory to other transitions in $MnF_2$ and to other magnetic materials is briefly discussed.

## I. INTRODUCTION

THE optical and far-infrared spectra of magnetically ordered materials have been under intensive investigation in recent years.[1] For the most part these spectra have been interpreted within the framework of crystalline-field theory by assuming that the magnetic (exchange) interactions effecting a single ion can be replaced by an average magnetic field. This so-called molecular-field approximation has been fairly successful in explaining line shifts and line splittings which occur in some materials below the ordering temperature. However, phenomena such as the appearance of extra lines[2,3] and anomalous intensity changes[4] below the ordering temperature are not adequately explained by this simple theory. The extension of the theory by Sugano and Tanabe[1] to include the fluctuations in the exchange field was only moderately successful in explaining the anomalous phenomena.

In most of these early optical studies, no attempt was made to consider in detail the collective excitations, i.e., the spin waves (magnons) and excitons. The work of Sievers and Tinkham,[5] and Richards[6] in the far infrared is an exception. They measured the exchange resonances of many magnetic materials and were able to predict the positions, temperature shifts, and magnetic field behavior of these resonances on the basis of spin-wave theory. Other authors[3,7,8] have considered the effects of magnons and excitons in optical spectra. However, this work has been of a more qualitative nature.

Within the past two years, several experiments have been performed which have conclusively demonstrated the importance of spin waves and excitons in the spectra of magnetic materials. Halley and Silvera[9] in antiferromagnetic $FeF_2$ and Allen, Loudon, and Richards[10] in antiferromagnetic $MnF_2$ have found far-infrared transitions which have been interpreted as two-magnon absorption. Greene, *et al.*,[11] have shown that a transition in the visible spectrum of $MnF_2$ is a spin-wave sideband (exciton-magnon absorption). The sideband indentification in $MnF_2$ has been confirmed by magnetic field[12,13] and stress[14] studies. In addition, more recent work has identified spin-wave sidebands in other magnetic materials[13,15–17] and Raman scattering from spin waves in $FeF_2$ has been observed.[18]

* Work supported in part by the National Aeronautics and Space Administration under Grant No. NsG 331 and in part by the Advanced Research Projects Agency through the Stanford Materials Research Center.

† National Science Foundation Predoctoral Fellow 1965–66. Present address: Bell Telephone Laboratories, Murray Hill, New Jersey.

‡ Early phases of this work were carried out at the University of California, at Berkeley with support from the National Science Foundation.

[1] For a good review of the early work in this field see S. Sugano and Y. Tanabe, in *Magnetism*, edited by G. T. Rado and H. Suhl (Academic Press Inc., New York, 1964), Vol. I, Chap. 6; K. Wichersheim, *ibid*, Chapter 7.

[2] K. Knox, R. G. Shulman, and S. Sugano, Phys. Rev. **130**, 512 (1963).

[3] R. Newman and R. M. Chrenko, Phys. Rev. **114**, 1507 (1959).

[4] T. Tusjikawa and E. Kanda, J. Phys. Soc. Japan. **18**, 1382 (1963).

[5] A. J. Sievers and M. Tinkham, Phys. Rev. **129**, 1995 (1963).

[6] P. L. Richards, J. Appl. Phys. **34**, 1237 (1963).

[7] A. I. Belyaeva and V. V. Eremenko, Zh. Eksperim. i Teor. Fiz. **44**, 469 (1963) [English transl.: Soviet Phys.—JETP **17**, 319 (1963)]; V. V. Eremenko and A. I. Belyaeva, Fiz. Tverd. Tela **5**, 2877 (1964) [English transl.: Soviet Phys.—Solid State **5**, 2106 (1964)]; V. V. Eremenko, Y. A. Popkov, and Y. G. Litvinenko, Zh. Eksperim. i Teor. Fiz. **47**, 1733 (1965) [English transl.: Soviet Phys.—JETP **20**, 1165 (1965)].

[8] G. S. Krinchik and G. K. Tyutneva, Zh. Eksperim. i Teor. Fiz. **46**, 435 (1964) [English transl.: Soviet Phys.—JETP **19**, 292 (1964)].

[9] J. Woods Halley and I. Silvera, Phys. Rev. Letters **15**, 654 (1965); Phys. Rev. **149**, 415 (1966); **149**, 423 (1966).

[10] S. J. Allen Jr., R. Loudon, and P. L. Richards, Phys. Rev. Letters **16**, 463 (1966).

[11] R. L. Greene, D. D. Sell, W. M. Yen, A. L. Schawlow, and R. M. White, Phys. Rev. Letters **15**, 656 (1965).

[12] D. D. Sell, R. L. Greene, W. M. Yen, A. L. Schawlow, and R. M. White, J. Appl. Phys. **37**, 1229 (1966).

[13] P. G. Russell, D. S. McClure, and J. W. Stout, Phys. Rev. Letters **16**, 176 (1966).

[14] R. E. Dietz, A. Misetich, and H. J. Guggenheim, Phys. Rev. Letters **16**, 841 (1966).

[15] L. F. Johnson, R. E. Dietz, and H. J. Guggenheim, Phys. Rev. Letters **17**, 13 (1966).

[16] R. Stevenson, Phys. Rev. **152**, 531 (1966).

[17] D. S. McClure, Proceedings of the Conference on Optical Properties of Ions in Crystals, Johns Hopkins University, 1966 (to be published).

[18] P. A. Fleury, S. P. S. Porto, L. E. Chessman, and H. J. Guggenheim, Phys. Rev. Letters **17**, 84 (1966).

TABLE I. Properties[a] of the ${}^6A_{1g}$ to ${}^4T_{1g}({}^4G)$ sharp-line absorption spectrum in $MnF_2$ at 2.2°K.

| Line | Position at 2.2°K ($cm^{-1}$) | Position at 2.2°K (Å) | Dipole character | Peak-absorption strength ($cm^{-1}$) | Oscillator strength | Full width at half-maximum ($cm^{-1}$) |
|---|---|---|---|---|---|---|
| $E1$ | 18 418.35±0.06 | 5427.86 | $M$ | 0.71 | $1.2\times10^{-11}$ | 0.49 |
| $E2$ | 18 435.30±0.06 | 5422.87 | $M$ | 0.45 | $8.7\times10^{-12}$ | 0.58 |
| $\pi1$ | 18 460.01±0.16 | 5415.61 | $E$ | 1.7 | $7.1\times10^{-11}$ | 12.0 |
| $\sigma1$ | 18 475.77±0.10 | 5410.99 | $E$ | 3.0 | $4.7\times10^{-11}$ | 3.2 |
| $\sigma2$ | 18 483.97±0.13 | 5408.59 | $E$ | 3.3 | $6.8\times10^{-11}$ | 5.0 |

[a] In the previously reported data (Refs. 11 and 12) the relative positions of the lines were correct; however, the absolute positions were incorrect because of a calibration error.

Two possible interactions have been proposed to explain these phenomena. Halley and Silvera[9] ascribe the interaction to an odd-parity crystalline field produced at one ion due to the spin-dependent electric quadrupole moments of the neighboring ions. Tanabe, Moriya, and Sugano[19] proposed a mechanism coming from a combined effect of atomic electric dipole moments and off-diagonal exchange interactions. Both theories are special cases of an earlier theory proposed by Dexter[20] to explain the electric dipole absorption by pairs of ions first observed by Varsanyi and Dieke[21] in $PrCl_3$.

In this paper we extend and discuss in more detail our work on the optical absorption in $MnF_2$. Brief accounts of some of this work have been given previously.[11,12,22] The room-temperature optical absorption spectrum of $MnF_2$ is shown[23] in Fig. 1. In this paper we shall restrict ourselves to the ${}^6A_{1g}$ to ${}^4T_{1g}({}^4G)$ absorption. The sharp structure for this transition at 2.2°K is shown in Fig. 2. The properties of the fine structure lines are summarized in Table I. In Ref. 11 we showed that the lines labeled $E1$ and $E2$ are pure electronic transitions. The band $\sigma1$ was shown to be a spin-wave sideband (exciton-magnon absorption) associated with $E1$. This association was based on the shape, temperature-dependent shift, and position of $\sigma1$ relative to $E1$. In this paper we show that $\pi1$ and $\sigma2$ are also spin-wave sidebands. In Ref. 12 we described the magnetic field behavior of these lines. A single-ion model was proposed to explain the results and an excited-state $g$ value was obtained.

This paper is organized as follows: First (Sec. II) the experimental results are presented. Next, the theory is developed (Secs. III to VI) and a detailed discussion of the experimental results is given (Sec. VII). In Sec. III a detailed crystal-field calculation is carried out which enables us to identify the two magnetic dipole lines $E1$ and $E2$. In Sec. IV the nature of the Frenkel excitions in $MnF_2$ is discussed. The spin-wave properties of $MnF_2$, as they apply to our problem, are discussed in Sec. V. The interaction leading to the exciton-magnon process is discussed in Sec. VI. Basically, this is an elaboration of earlier work with particular emphasis on the collective nature of the excitations. The symmetry of the excitons and magnons is determined and employed to determine the selection rules for the sideband absorption. In Sec. VII we give a detailed discussion of the shape, stress dependence, temperature dependence and Zeeman behavior of the sidebands $\pi1$, $\sigma1$, and $\sigma2$. In Sec. VIII we briefly consider the application of our results to sidebands in other systems.

## II. EXPERIMENTAL DETAILS

### A. Procedures and Apparatus

Single crystals of $MnF_2$ were grown at Stanford University by R. Feigelson. Manganese metal (cation impurities less than 34 ppm) was reacted with hydrofluoric acid to produce $MnF_2$ powder which was then melted in an HF atmosphere. This feed material was transferred to a vacuum-baked, high-purity graphite crucible and was grown by a modified Bridgman technique under a steep temperature gradient in a purified argon atmosphere. Crystals were also obtained from Semi-Elements. Semiquantitative spectroscopic analysis by American Spectrographic Laboratories indicated that no cation impurities were present in concentrations greater than 100 ppm in any of the samples used for these experiments. For such crystals the absorption spectrum did not exhibit any sample dependence. A 7-mm absorption path was used to obtain the spectrum shown in Fig. 2.

Absorption measurements were made by shining light from a PEK X-76 high-pressure, xenon short arc lamp through the crystal onto the slits of a spectrometer. A Spex model 1700 scanning spectrometer was used in first order for line-shape studies. Signals were detected by an EMI 9558 (S-20) photomultiplier. A Jarrell-Ash 1-m Ebert scanning spectrometer was used in tenth order, and a Bausch and Lomb dual grating spectrograph in first order to accurately measure line positions. Line positions on the spectroscopic plates were measured

[19] Y. Tanabe, T. Moriya, and S. Sugano, Phys. Rev. Letters **15**, 1023 (1965).
[20] D. L. Dexter, Phys. Rev. **126**, 1962 (1962).
[21] F. Varsanyi and G. H. Dieke, Phys. Rev. Letters **7**, 442 (1961).
[22] R. L. Greene, D. D. Sell, and R. M. White, Proceedings of the Conference on Optical Properties of Ions in Crystals, Johns Hopkins University, 1966 (to be published).
[23] Data of J. W. Stout, J. Chem. Phys. **31**, 709 (1959).

with a Grant comparator. Standard reference lines were superimposed on the spectra for calibration. The resolution was approximately 0.1 $cm^{-1}$ and the line positions could be determined to approximately $\pm 0.1$ $cm^{-1}$.

For temperatures below 4.2°K the sample was immersed in liquid helium. Sample temperatures between 4.2 and 77°K were obtained by boiling liquid helium in a storage Dewar and blowing the cold helium gas over the sample. Stable temperatures ($\pm 0.2$°K) were maintained for several minutes by controlling the electrical power used to boil the helium. Temperatures below 20°K were measured with a carbon resistor to an accuracy of $\pm 0.1$°K; temperatures above 20°K were measured with a copper versus gold-cobalt[24] thermocouple to an accuracy of $\pm 0.2$°K. In each case the temperature sensing element was glued to the sample with General Electric 7031 varnish.

Oriented samples were used for the polarization studies. Since $MnF_2$ is birefringent it was quite easy to accurately align the polarizer by using the sample as a wave plate between two crossed polarizers. Polarization discrimination of better than 100 to 1 was obtained.

### B. Experimental Results

As mentioned in the Sec. I, we shall concentrate upon the five spectral lines shown in Fig. 2. This is the sharp line structure at 2.2°K of transitions from the ${}^6A_{1g}$ ground state to the lowest-${}^4T_{1g}({}^4G)$ excited state for a 7-mm thick single crystal of $MnF_2$. The lines are strongly polarized. Four lines, $E1$, $E2$, $\sigma 1$, and $\sigma 2$ appear in $\sigma$ polarization ($\mathcal{E} \perp c$, $\mathcal{H} \parallel c$), and $\pi 1$ appears in $\pi$ polarization ($\mathcal{E} \parallel c$, $\mathcal{H} \perp c$). Here $\mathcal{E}$ and $\mathcal{H}$ are the electric and magnetic vectors of the light and $c$ is the optic axis of the crystal ($z$ axis). In $\alpha$ polarization ($\mathcal{E} \perp c$, $\mathcal{H} \perp c$), only lines $\sigma 1$ and $\sigma 2$ are observed. Thus, for lines $\pi 1$, $\sigma 1$, and $\sigma 2$ the electric vector of the light must be the important perturbation and these are electric-dipole transitions. Similarly, we see that the optical-magnetic field direction determines the properties of $E1$ and $E2$, thus, these are magnetic-dipole transitions. The properties of these lines are summarized in Table I.

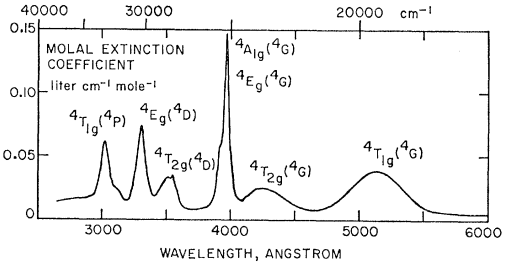


FIG. 1. Absorption spectrum of $MnF_2$ at room temperature. The excited cubic crystal-field states for the respective transitions are shown. (After J. W. Stout, Ref. 23).

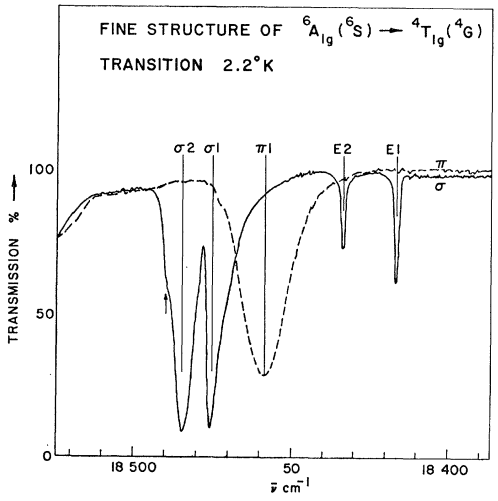


FIG. 2. Sharp line structure of ${}^6A_{1g}$ to ${}^4T_{1g}$ absorption at 2.2°K. The solid and dashed curves denote $\sigma$ and $\pi$ polarizations, respectively.

As the temperature increases the peak-absorption strengths decrease and the lines broaden and shift. The broadening of $E1$ and $E2$ is especially severe. The widths increase from approximately 0.5 $cm^{-1}$ at 2.2°K to approximately 8 $cm^{-1}$ at 30°K and the peak absorption becomes so weak that the line positions cannot be determined accurately.[25] Lines $\pi 1$, $\sigma 1$, and $\sigma 2$ do not change as drastically with temperature but become too weak to be observed at approximately 65°K. However, at approximately 33°K, lines $\sigma 1$ and $\sigma 2$ coalesce into a single broad line, thus 30°K is a practical upper temperature limit for high-resolution studies of these lines. The temperature shift of lines $E1$ and $E2$ has also been studied by Yen, Imbusch, and Huber.[25] The shifts of $\pi 1$, $\sigma 1$, and $\sigma 2$ relative to $E1$ and $E2$ are discussed in detail in Sec. VII.C.

In a 10.0-kOe field parallel to the $z$ axis lines $E1$ and $E2$ split by $1.71 \pm 0.05$ $cm^{-1}$; lines $\pi 1$, $\sigma 1$, and $\sigma 2$ show no apparent splitting or shifting. Both lines $E1$ and $E2$ split into equal intensity components which are symmetrical about the zero-field positions to within our experimental accuracy. Fields of comparable strength applied perpendicular to the $z$ axis have no effect upon any of these lines.

## III. CRYSTAL-FIELD THEORY

### A. Crystal Field in $MnF_2$

In this section we consider the effect of the crystalline field upon the energy levels of the $Mn^{2+}$ ion. Our motivation for this is to explain the existence and characteristics of lines $E1$ and $E2$ and to determine the

[24] R. L. Powell, M. D. Bunch, and R. J. Corruccini, Cryogenics **1**, 139 (1961).

[25] W. M. Yen, G. Imbusch, and D. Huber (to be published).

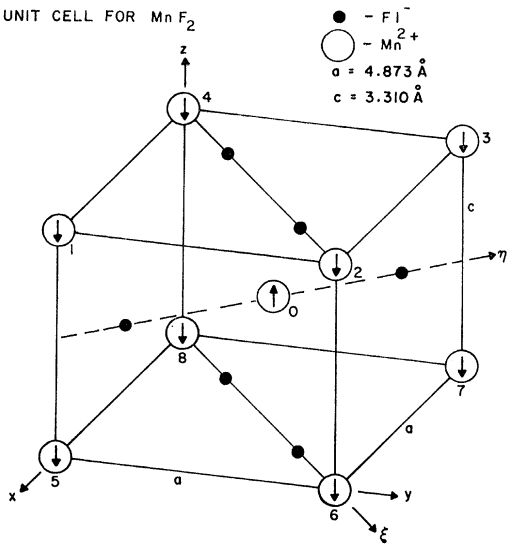


FIG. 3. The unit cell for $MnF_2$ (rutile structure). The body-centered ion is on sublattice 1, while the corner ions are on sublattice 2.

nature of the excited states which enter into our discussions of the sidebands.

The optical properties of $MnF_2$ arise from the five $3d$ electrons of the $Mn^{2+}$ ion. This $3d^5$ configuration gives rise to an array of 252 states consisting of one sextuplet and various quartets and doublets. Due to the Coulomb interaction among the $3d$ electrons, these states are split into various terms.

The $MnF_2$ has a rutile crystal structure as shown in Fig. 3. The $Mn^{2+}$ ions form two interpenetrating simple tetragonal sublattices, each characterized by an environment rotated by 90° about the $z$ axis with respect to the other sublattice. The neighboring fluorine ions produce a crystalline electric field at the $Mn^{2+}$ site which is predominantly of cubic symmetry. This cubic field mixes and splits the terms into representations of the octahedral group. The strength of this field is expressed in the usual manner in terms of the parameter $Dq$. By comparing the resulting eigenvalues with the observed spectrum in Fig. 1, it is found that $Dq$ is approximately 900 $cm^{-1}$.

Let us now concentrate upon the ${}^6A_{1g}$ ground state and the lowest-${}^4T_{1g}$ excited state. In terms of the free-ion states, the twelve degenerate eigenfunctions of the ${}^4T_{1g}$ state have the form[26]

$$\begin{aligned}{}^4T_{1g}(1, M_s) = N[&\sqrt{\tfrac{1}{8}}\,{}^4G(-3, M_s) + \sqrt{\tfrac{7}{8}}\,{}^4G(1, M_s) \\ &- \alpha_P {}^4P(1, M_s) + \sqrt{\tfrac{5}{8}}\alpha_F {}^4F(-3, M_s) \\ &+ \sqrt{\tfrac{3}{8}}\alpha_F {}^4F(1, M_s)], \qquad (3.1)\end{aligned}$$

with similar expressions for ${}^4T_{1g}(0, M_s)$ and ${}^4T_{1g}(-1, M_s)$; here $M_s = \pm\frac{3}{2}, \pm\frac{1}{2}$. The admixture coefficients are proportional to the cubic-field parameter, $Dq$. Using the value $Dq = 900$ $cm^{-1}$ the coefficients become $N = 0.792$, $N\alpha_P = 0.594$, and $N\alpha_F = -0.140$. The corresponding eigenvalue is 17 256 $cm^{-1}$. Notice that we are using the so-called weak-field scheme. We are doing this in order to take advantage of the results of Ref. 26.

In addition to the Coulomb interaction and the cubic-crystal field there are also a spin-orbit coupling, an exchange interaction, and lower symmetry components to the crystal field. The spin-orbit interaction has the form $\zeta^* \sum_i \mathbf{l}_i \cdot \mathbf{s}_i$ where $\zeta^*$ is taken[27] to be about 260 $cm^{-1}$. We shall represent the exchange interaction in this section by a molecular field. Thus, the interaction is written $\pm 2\beta H_E S_z$, the sign depending upon the sublattice the $Mn^{2+}$ ion belongs to. If the $Mn^{2+}$ ion under consideration as well as its neighboring ions are all in their ground states $2\beta H_E = 56$ $cm^{-1}$. If the ion under consideration is in an excited state while its neighbors are still in their ground state, the exchange is taken to be $2\beta H_E = 67$ $cm^{-1}$. This latter value is obtained from the data of Yen, Imbusch, and Huber.[25]

The symmetry of the fluorine ions about a $Mn^{2+}$ ion site is $D_{2h}$. The six fluorine ions are equidistant from the $Mn^{2+}$ ion. However, the bonds in the $\xi$-$z$ plane (for sublattice 1) are twisted from the 90° cubic configuration to 78° thereby introducing an orthorhombic crystalline field.

The combined effect of spin orbit, molecular field, and orthorhombic field on the ${}^4T_{1g}$ state is extremely complicated. In order to make our problem more tractable, we shall restrict ourselves to the 12 states of this ${}^4T_{1g}$ manifold. This neglects coupling with the higher-lying states. Even though they are several thousand wave numbers away, their effect may be important. Clogston[26] has already obtained the 12 eigenfunctions of this manifold including cubic field and the spin-orbit interaction. He finds that the ${}^4T_{1g}$ splits into four double-group representations $\Gamma_6$, $\Gamma_7$, $\Gamma_8$, and $\Gamma_8'$. The corresponding eigenvalues and eigenfunctions are given in Table 4 of Clogston's paper.

It can be shown that within the ${}^4T_{1g}$ manifold the orthorhombic potential can be expressed in terms of a many-electron equivalent operator

$$V_{D_{2h}} = C_1(\Gamma_z^2 - \tfrac{2}{3}) + C_2(\Gamma_\xi^2 - \Gamma_\eta^2), \qquad (3.2)$$

where the operators $\Gamma_\xi$, $\Gamma_\eta$, and $\Gamma_z$ act on the components of the triplet in a manner completely analogous to the operation of orbital angular momentum operators on states characterized by $L$ and $M_L$. It is in this sense that the triplet may be treated as an effective $L = 1$ state as was done by Dietz, Misetich, and Guggenheim.[14] It should be pointed out that the expression in Eq. (3.2) is not unique. The only restriction is that it be invariant under the symmetry operations of $D_{2h}$. For example, the expression with $\xi$ and $z$ interchanged

[26] A. M. Clogston, J. Phys. Chem. Solids **7**, 201 (1958).

[27] Since $Mn^{2+}$ has a half-filled shell the first-order spin-orbit coupling within a given term vanishes. The coupling in the ${}^4T_{1g}$ state is not completely quenched because it is formed from $P$, $F$, and $G$ free-ion terms and there is coupling between different terms ($\zeta \sim 400$–$500$ $cm^{-1}$). We account for this by using the effective coupling $\zeta^* = 260$ $cm^{-1}$.

would be equally good. If we use this latter convention and replace $\Gamma_\mu$ by $L_\mu$, our Hamiltonian agrees with that of Dietz, *et al.* Our coefficients in Eq. (3.2) are related to theirs by $C_1=(3\Gamma+\Delta)/2$ and $C_2=(\Gamma+\Delta)/2$.

Collecting the three terms, the effective Hamiltonian for the $^4T_{1g}$ state for an ion on sublattice 1 is

$$\mathcal{H}=-2\beta H_E S_z+\mathcal{H}_{s-o}+C_1(\Gamma_z^2-\tfrac{3}{2})+C_2(\Gamma_\xi^2-\Gamma_\eta^2). \quad (3.3)$$

Although we have values for the exchange field and the spin-orbit coupling it is difficult to obtain independent estimates of $C_1$ and $C_2$. Thus, we must adjust $C_1$ and $C_2$ to obtain eigenstates which account for the observed properties of lines $E1$ and $E2$.

### B. Lines $E1$ and $E2$

We are concerned with transitions from the $^6A_{1g}$ to $^4T_{1g}$. We begin by considering the $^6A_{1g}$ state. In lowest order the orthorhombic field does not affect this state since it is an orbital singlet. The spin-orbit coupling between the levels of this multiplet vanishes for the same reason ($L=0$). The exchange-field splits the state into its six $S_z$ components. Therefore, for sublattice 1 the ground state is $^6A_{1g}(\frac{5}{2})$ and for sublattice 2 it is $^6A_{1g}(-\frac{5}{2})$. These levels are denoted by $|g\rangle$ in Fig. 5. [The levels denoted by $|m\rangle$ are the $^6A_{1g}(\frac{3}{2})$ and $^6A_{1g}(-\frac{3}{2})$ levels for the two sublattices.]

The transitions between $^6A_{1g}$ and $^4T_{1g}$ are electric-dipole forbidden because both states have even parity. They are also spin forbidden ($S=\frac{5}{2}$ to $S=\frac{3}{2}$) but this is relaxed by spin-orbit coupling between the ground and excited states. Since only the $^4T_{1g}(1,\frac{3}{2})$ couples to $^6A_{1g}(\frac{5}{2})$, the ground state[28] for sublattice 1 (considering only the lowest-lying $^4T_{1g}$ state) is

$$|g\rangle=|\,^6A_{1g}(\tfrac{5}{2})\rangle+(\sqrt{2}\zeta/\Delta E)\,|\,^4T_{1g}(1,\tfrac{3}{2})\rangle. \quad (3.4)$$

[We shall discuss the results for sublattice 1. The corresponding results for sublattice 2 are quite obvious.] Using the spin-orbit parameter $\zeta\sim 400$ cm$^{-1}$ and $\Delta E=18\,400$ cm$^{-1}$, we see that the admixture of $^4T_{1g}(1,\frac{3}{2})$ into $|g\rangle$ is approximately 0.03. The fact that this mixing is rather small will be important when we discuss the mechanisms which cause sidebands in Sec. VI. This also gives an indication why the observed lines are so weak.

Bearing in mind that the optical magnetic perturbation is $\beta\mathcal{H}\cdot(\mathbf{L}+2\mathbf{S})$, it is not difficult to see that for sublattice 1 the strength of the $\sigma$-polarized lines ($\mathcal{H}\,||\,c$) is proportional to the $^4T_{1g}(1,\frac{3}{2})$ admixture in the excited states and that $\pi$ lines depend upon admixtures of $^4T_{1g}(0,\frac{3}{2})$ or $^4T_{1g}(1,\frac{1}{2})$. By using the Hamiltonian in Eq. (3.3) and Clogston's basis functions it is found that the twelve states of $^4T_{1g}$ decouple into the two sets, one leading to $\sigma$ lines, the other to $\pi$ lines. In general, there could be six magnetic dipole lines in the $\sigma$ spectrum and also six in the $\pi$ but no line can appear in both polarizations. In the actual spectrum only two lines in $\sigma$ polarization are strong enough to be observed. There are two factors affecting the observed strength: (1) The parameters in the Hamiltonian may be such that the transition strength is small for some eigenstates, i.e., small admixture of $|1,\frac{3}{2}\rangle$. (2) Some excited states may be so broad, because of lifetime broadening for example, that the transitions are not detected.

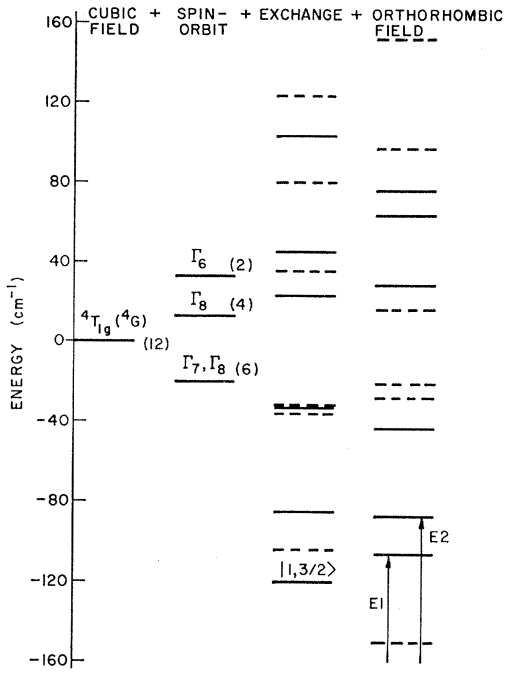


FIG. 4. Splitting of the $^4T_{1g}$ state in $MnF_2$. The levels denoted by solid lines are coupled to the ground state by $\sigma$-polarized ($\mathcal{H}\,||\,z$) transitions. Those denoted by dashed lines couple in $\pi$ polarization.

Using Eq. (3.3) and Clogston's wave functions as a basis, we have diagonalized the two $6\times6$ submatrices for various values of the parameters $C_1$ and $C_2$. The results for $C_1=70$ cm$^{-1}$ and $C_2=18$ cm$^{-1}$ shown in Fig. 4 are in reasonably good agreement with observation. For these parameters there are two lines in $\sigma$ polarization separated by 17 cm$^{-1}$ with an intensity ratio ($E1$ to $E2$) of 4. The observed intensity ratio is 1.3. We must be cautious in ascribing significance to these numerical values, since we have neglected effects which will alter the quantitative results. It is significant though that the excited states which are observed are near the bottom of the twelve-level manifold, with the state for $E1$ being the lowest lying excited state for $\sigma$ polarization.

In their stress studies Dietz, Misetich, and Guggenheim[14] considered only the $2\times2$ submatrix of $|1,\frac{3}{2}\rangle$ and $|-1,\frac{3}{2}\rangle$ which are coupled by the orthorhombic field and neglected the (first order) mixing via spin-orbit coupling. They found that this model was adequate to explain their stress results. We have pursued

[28] R. M. Macfarlane (private communication).

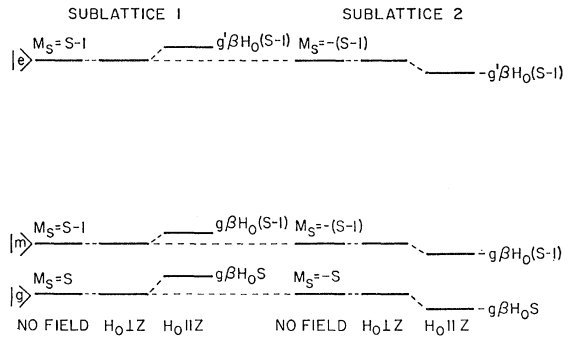


FIG 5. The effect of an external magnetic field $H_0$ upon the single-ion energy levels.

the larger problem in order to obtain some idea of the nature of the other states in the $^4T_{1g}$ manifold.

For our discussions we shall assume that $|e\rangle$ has $M_s=\frac{3}{2}$. This is not a poor approximation since it is the $|1, \frac{3}{2}\rangle$ character of the excited state $|e\rangle$ which causes the transitions $E1$ and $E2$.

We should briefly note that the observed lines $E1$ and $E2$ are quite narrow, being approximately 0.5 $cm^{-1}$ wide at 2.2°K. It is rather unusual for a pure material to exhibit such sharp lines. The width that is observed can be attributed to two sources: (1) Local strains within the crystal cause inhomogeneous broadening that probably accounts for most of the width at 2.2°K. Experimentally, it is found that the width is slightly crystal dependent and that it can be decreased by careful crystal preparation. (2) The finite lifetime of the ionic states leads to homogeneous broadening. Yen, *et al.*,[25] have studied the temperature dependence of the width of these lines; they find that the lines broaden quite rapidly as the temperature is increased and that this broadening results from a magnon Raman process which is the analog of the familiar phonon Raman broadening. [The reason why $E2$ is broader than $E1$ at 2.2°K may be that $|e(E2)\rangle$ is lifetime-broadened by a direct phonon or magnon transition to $|e(E1)\rangle$.]

It is important that these pure transitions are sharp lines for it is their width that determines the sensitivity with which we can "probe" the system. For example, the sidebands lose their sharp features as the temperature is increased. It is the broadening of the excited state which causes this loss of resolution.

Let us now consider the Zeeman splitting of these lines. Unlike the usual case in a nonmagnetic system where a magnetic field lifts degeneracies within the ion, the levels in a magnetic crystal are already nondegenerate. The observed line-splitting results because the magnetic field affects the two sublattices differently as shown in Fig. 5. At present we are concerned with the two states $|g\rangle$ and $|e\rangle$ where we use the latter symbol to denote either of the two final states associated with lines $E1$ and $E2$.

In a field perpendicular to the $z$ axis, $|g\rangle$ and $|e\rangle$ are unaffected and the transition energies are unchanged. The linear shifts depend upon the matrix elements of the form $\langle e|L^{\pm}+2S^{\pm}|e\rangle$. By inspecting the six functions for $\sigma$ polarization, we find that all such matrix elements vanish. The similar diagonal matrix elements of $|g\rangle$ also vanish. The state $|e\rangle$ could show a small quadratic field dependence due to second-order coupling (to the six $\pi$ polarization states); however, this is not observed.

For an external field parallel to the $z$ axis we define a $g$ value in terms of the level shift

$$\beta H_0\langle i|L_z+2S_z|i\rangle\equiv g^i\beta H_0\langle i|S_z|i\rangle. \quad (3.5)$$

It is easily seen from Fig. 5 that the lines should split symmetrically about the zero-field position, as is observed, and should split by an amount

$$\Delta_1=2\beta H_0|gS-g'(S-1)|. \quad (3.6)$$

Assuming a ground state[29] $g=2.00$ and using the observed splitting of $1.71\pm0.05$ $cm^{-1}$ in a 10.0 kOe field, we obtain[30] $g'=2.11\pm0.04$ for both $E1$ and $E2$. For the crystal-field parameters used the calculated value is approximately 2.4.

This completes our discussion of the lines $E1$ and $E2$ except for one point. We have taken account of the different circumstances for ions on the two sublattices, but we have not considered the fact that all the ions on a sublattice are equivalent and that the excitation may hop from one ion to another. This is discussed in Sec. IV where it is shown that the single-ion description of lines $E1$ and $E2$ is justified (because of special circumstances in $MnF_2$).

## IV. EXCITON THEORY

The concept of excitons is not a familiar one in the study of sharp optical spectra of transition-metal ions in solids. The main reason for this is that usually the transition metal ion, call it the active ion, is imbedded in a host material having no optical structure in the region of study. It is meaningful to speak of exciting a *single* ion since the active ion cannot easily transfer its energy to the rest of the crystal.

In crystals with higher concentrations of active ions, pair effects become important. For example, in concentrated ruby,[31] coupled near-neighbor pairs of $Cr^{3+}$ ions cause new structure and in $KZnF_3$ pairs[32] of $Mn^{2+}$ ions give rise to absorption lines much stronger than those of the single ions. For such systems it is meaningless to speak of single-ion excitations. The two ions are coupled so strongly that if one ion is initially

[29] The value $g=2.00$ for the ground state of $Mn^{2+}$ in $ZnF_2$ has been measured by M. Tinkham [Proc. Roy. Soc. (London) **A236**, 535 (1956)]. We expect the same value for the ground state in $MnF_2$.

[30] This value depends upon the assignment $M_s=3/2$ for the state $|e\rangle$.

[31] A. L. Schawlow, D. L. Wood, and A. M. Clogston, Phys. Rev. Letters **3**, 271 (1959).

[32] J. Ferguson, H. J. Guggenheim, and Y. Tanabe, J. Appl. Phys. **36**, 1046 (1965); Phys. Rev. Letters **14**, 737 (1965); J. Phys. Soc. Japan **21**, 692 (1966).

excited it quickly shares the excitation with the other ion and consequently we speak of excited states of the *pair*. The strength of the coupling is the criterion for determining when two ions must be treated as a pair. Typically, coupling energies greater than a few wave numbers will lead to observable optical effects.

In the limiting case of a pure crystal we cannot speak of single ions or of pairs. We must consider the collective excitations of the whole crystal, i.e., excitons. There are two limiting approximations of excitons.[33] In the weak-binding limit we have the Wannier excitons. These are bound electron-hole pairs which can propagate. The other limiting case is the one we are concerned with in this study. This is the tight-binding approximation in which the binding within the ion is much greater than the binding between ions. This is usually referred to as a Frenkel exciton. Unlike the Wannier exciton, the electrons remain tightly bound to a given ion and it is the ionic excitation that propagates. Since the inter-ion coupling is relatively small, the optical spectra of such systems are usually qualitatively similar to the corresponding spectra of dilute crystals. Nevertheless, there are significant differences which we shall discuss in the following sections.

Before we continue, let us briefly digress to describe the Brillouin zone in crystals with the rutile structure. The unit cell shown in Fig. 3 is also the primitive Bravais lattice because both the body-centered ion and a corner ion are associated with one lattice point. Thus, the generators of reciprocal space are $\mathbf{a}_1^*=\hat{x}2\pi/a$, $\mathbf{a}_2^*=\hat{y}2\pi/a$, and $\mathbf{a}_3^*=\hat{z}2\pi/c$ and the Brillouin zone is a simple tetragonal cell with corners at $\pm\pi/a$, $\pm\pi/a$, $\pm\pi/c$. We note that this is still true in the ordered magnetic state. In other words, the chemical primitive cell is also the magnetic primitive cell.

### A. Simple Exciton Model

We first consider a simple model[34] for Frenkel excitons which will illustrate their basic properties. This will also provide a basis for our discussion of excitons in $MnF_2$ and will introduce the formalism which we will use to describe the exciton-magnon interaction. We shall not attempt to treat this problem with complete rigor, for such a discussion would be beyond the scope of this work.

The various methods of handling the inter-ion coupling in systems such as $MnF_2$ are discussed by Anderson[35] in his work in superexchange, which is a rather similar problem. He points out that it is very important to begin with the proper single-ion wave functions which, in this case, are products of one-electron Wannier functions. This effectively separates the problem into two parts. The first part is a complicated ligand field problem of finding the wavefunctions of a magnetic ion including all crystalline interactions except the interactions between the magnetic ions. In principle, this can be done by forming the Wannier functions from Bloch functions which are themselves solutions to the Hartree-Fock equation. The effects of the nonmagnetic intervening ions are included here. Since we shall not be concerned with the detailed nature of the wave function, we shall assume that this portion of the problem has been solved and that it has yielded the wave functions which we introduce below. We can think of the wave functions discussed in Sec. III as zero-order approximation to these Wannier wave functions. The remaining problem of the interaction between the magnetic ions is now greatly simplified, since the complicated ligand-field effects have been included in the wave functions.

We shall use a formalism appropriate for crystals with rutile structures. We consider a crystal with periodic boundary conditions containing $N$-unit cells. Each cell contains two inequivalent magnetic ions (as well as the nonmagnetic intervening ions) at centers of symmetry, and each magnetic ion has $h$ optically active electrons. We further assume that the crystal is rigid and we thus ignore the effects of phonons.

Suppose as a zero-order approximation that the ions do not interact and that each ion is described by a Hamiltonian $\mathcal{H}_{n\mu}$, where $n\mu$ refers to the $\mu$th ion site of the $n$th unit cell. Furthermore, assume that $\mathcal{H}_{n\mu}$ has only two eigenstates, a ground state $|\, g_{n\mu}\rangle$ and an excited state $|\, e_{n\mu}\rangle$.

Using the convention that capital letters refer to states of the crystal and small letters refer to single-ion states, the wave function of the ground state of the entire crystal is

$$|\, G\rangle = |\, A \prod_{n=1}^{N} \prod_{\mu=1}^{2} g_{n\mu}\rangle, \tag{4.1}$$

and that for the excited state in which the $n\mu$th ion is excited is

$$|\, E_{n\mu}\rangle = |\, A e_{n\mu} \prod_{j\nu \neq n\mu} g_{j\nu}. \tag{4.2}$$

The operator $A$ antisymmetrizes the crystal wave functions to insure that the exclusion principle is obeyed and that the electrons are indistinguishable. The initial single-ion wave functions dictate its form.

If we now include the interaction energy $V_{n\mu,j\nu}$ between the $n\mu$th and the $j\nu$th ions, the Hamiltonian for the entire crystal is

$$\mathcal{H}=\sum_{n=1}^{N}\sum_{\mu=1}^{2}\mathcal{H}_{n\mu}+\tfrac{1}{2}\sum_{n,j=1}^{N}\sum_{\mu,\nu=1}^{2}V_{n\mu,j\nu} \tag{4.3a}$$

or using a shorthand notation,

$$\mathcal{H}=\mathcal{H}_0+V, \tag{4.3b}$$

[33] D. L. Dexter and R. S. Knox, *Excitons* (Interscience Publishers, Inc., New York, 1965).

[34] See for example, A. S. Davydov, *Theory of Molecular Excitons* (McGraw-Hill Book Company, Inc., New York, 1962); or J. Jortner, S. A. Rice, and J. L. Katz, J. Chem. Phys. **42**, 309 (1965).

[35] P. W. Anderson, *Magnetism*, edited by G. T. Rado and H. Suhl (Academic Press Inc., New York, 1963), Vol. I.

where $V_{n\mu,n\mu}$ is defined to be zero. It is not necessary for this development to know the origin of the interaction $V$, however, the Coulomb interaction probably provides most of this coupling even though other mechanisms may also contribute. Such problems have been discussed recently by Gondaira and Tanabe.[36]

The form of this Hamiltonian clearly illustrates two shortcomings of the wave functions $|E_{n\mu}\rangle$. They do not possess the translational symmetry of the crystal, and they are not eigenstates of the Hamiltonian when the $V$ terms are included. The first problem is solved by introducing linear combinations of these wave functions called single-site, or sublattice, excitons

$$|E^{\mu}\mathbf{k}\rangle = N^{-1/2}\sum_{n=1}^{N}\exp(i\mathbf{k}\cdot\mathbf{r}_{n\mu})\,|E_{n\mu}\rangle, \tag{4.4}$$

which are irreducible representations of the translational symmetry group (i.e., Bloch functions). The vector $\mathbf{r}_{n\mu}$ denotes the position of the $n\mu$th ion, and $\mathbf{k}$ is a reciprocal lattice vector in the first Brillouin zone. In addition, these wave functions simplify the diagonalization of the Hamiltonian because states with different $\mathbf{k}$'s are not coupled. (We neglect the small coupling between the excited and ground states for $\mathbf{k}=0$.)

The matrix elements of the Hamiltonian are

$$\langle E^{\mu}\mathbf{k}\,|\,\mathcal{H}\,|\,E^{\nu}\mathbf{k}\rangle = \delta_{\mu\nu}W(E)+V_{\mu\nu}(\mathbf{k}), \tag{4.5}$$

where

$$W(E)=\langle E_{01}\,|\,\mathcal{H}\,|\,E_{01}\rangle \tag{4.6}$$

is the energy of the crystal when one ion is excited, and $W(E)$ contains the so-called band-shift energy. The diagonal term

$$V_{11}(\mathbf{k})=\sum_{n=1}^{N}\langle e_{n1}g_{01}\,|\,V_{n1,01}\,|\,\mathcal{P}g_{n1}e_{01}\rangle\cos(\mathbf{k}\cdot\mathbf{r}_{n1}) \tag{4.7}$$

and the off-diagonal term

$$V_{12}(\mathbf{k})=\sum_{n=1}^{N}\langle e_{n2}g_{01}\,|\,V_{n2,01}\,|\,\mathcal{P}g_{n2}e_{01}\rangle\cos(\mathbf{k}\cdot\mathbf{r}_{n2}) \tag{4.8}$$

measure the excitation transfer between ions on the same sublattice and ions on opposite sublattices, respectively. From the invariance of the matrix elements in Eqs. (4.7) and (4.8) under inversion and translation it is easy to show that the $V_{\mu\nu}(\mathbf{k})$ are real and that $V_{12}(\mathbf{k})=V_{21}(\mathbf{k})$. For the rutile structure and the types of transitions that we are considering it is also true that $V_{11}(\mathbf{k})=V_{22}(\mathbf{k})$. This can be shown from symmetry arguments similar to those to be discussed in Sec. VI.

The $\mathcal{P}$ in these expressions is a permutation operator. For two-electron operators it leads to two types of matrix elements. In the direct term, the $2h$ electrons in the bra and the ket have the same arbitrary positions. In the exchange terms (there are $h^2$ such terms) one pair of electrons is interchanged between the ion sites and a minus sign is introduced.

Hence, Eq. (4.5) reduces to a $2\times2$ matrix for each value of $\mathbf{k}$. The eigenvalues give the exciton band energies

$$W^{\pm}(\mathbf{k})=W(E)+V_{11}(\mathbf{k})\pm V_{12}(\mathbf{k}), \tag{4.9}$$

while the exciton wave functions are

$$|E^{\pm}\mathbf{k}\rangle=\sqrt{2}^{-1}[|E^{1}\mathbf{k}\rangle\pm|E^{2}\mathbf{k}\rangle]. \tag{4.10}$$

The important points of this development are the following. The eigenstates, Eq. (4.10), are linear equally weighted combinations of sublattice excitons. The excitation is spread evenly throughout the crystal and it may be found with equal probability at any ion site. The eigenmodes, Eq. (4.9), form two $\mathbf{k}$ dependent bands reflecting the existence of two inequivalent types of ion sites. In general, the two bands are nondegenerate if $V_{12}(\mathbf{k})$ does not vanish. The splitting between the bands for $\mathbf{k}=0$, called the Davydov splitting, is twice the intersublattice coupling energy.

### B. Excitons in $MnF_2$

In this section we apply this exciton formalism to $MnF_2$. The ions in our model only have two energy levels. How can this model be applied to the $Mn^{2+}$ ion which has many excited states of the $3d^5$ configuration? As a first approximation we can neglect the coupling between nondegenerate ionic states which have energy separations large compared to the inter-ion coupling because the mixing between such states is small. In this approximation the exciton effects are treated independently for each excited state of the ion. This approximation is not completely justifiable for the exciton bands associated with lines $E1$ and $E2$ because these bands have nearly the same energy. Nevertheless, we are almost forced to accept it since higher-order approximations become exceedingly complicated.

In $MnF_2$ all the optical transitions of interest are spin-forbidden. For such transitions the intersublattice coupling $V_{12}(\mathbf{k})$ is vanishingly small. This can be seen intuitively from an argument given by Moriya.[37] For spin-forbidden transitions, the $z$ component of the total-spin-angular momentum changes by 2 when the excitation jumps from one sublattice to the other. Such a process requires spin-orbit coupling to the ground state, hence, with other things being equal, this coupling is relatively weak compared to the intrasublattice coupling.

The same conclusion is reached by estimating the magnitudes of $V_{11}(\mathbf{k})$ and $V_{12}(\mathbf{k})$. First of all consider the direct terms of Eqs. (4.7) and (4.8). Since the $Mn^{2+}$ ions are at centers of symmetry, the lowest multipole coupling (assuming $V$ is the Coulomb interaction) is quadrupole-quadrupole coupling. The matrix

[36] K. Gondaira, and Y. Tanabe, J. Phys. Soc. Japan **21**, 1527 (1966).

[37] T. Moriya, J. Phys. Soc. Japan **21**, 926 (1966).

elements include a spin sum as well as the spatial integration. Since $V$ is spin-independent, the spin sum dictates that the spin of each electron must be the same for the ground and excited states. To accomplish this, spin-orbit coupling between the ground and excited state must be invoked and the matrix elements are reduced by a factor of $[V_{so}/W(E)]^2$, or approximately $10^4$. Using arguments similar to Dexter's,[38] we estimate that the contributions of the direct interaction to $V_{11}$ and $V_{12}$ are much smaller than one wave number.

The exchange terms must be treated differently for inter- and intrasublattice coupling. Spin-orbit coupling must be invoked to satisfy the spin sum for $V_{12}$ but not for $V_{11}$; hence, we expect $V_{11}$ to be larger than $V_{12}$ by approximately the factor given above. It is reasonable to expect the exchange contribution of $V_{11}$ to be comparable to the observed excited state exchange interactions of $Mn^{2+}$ pairs[32] which are typically a few wave numbers. To sum up, the coupling $V_{12}$ is vanishingly small, and the exchange contribution to $V_{11}$ is estimated to be a few wave numbers.

In this special case with $V_{12}=0$ the properties of the excitons are greatly simplified. The reason for this is that the sublattice excitons become eigenstates of the system. This is very important because the excitation only resides on equivalent sites whereas in the general case it is evenly distributed between the two inequivalent sublattices.

It is easily seen that there will be no observable exciton effects for pure electronic absorption such as lines $E1$ and $E2$. Since light has a very long wavelength on the atomic scale and since $\mathbf{k}$ is conserved, these are transitions which create $\mathbf{k}\sim 0$ excitons. There can be no Davydov splitting because $V_{12}(\mathbf{0})\sim 0$. The selection rules for absorption are the same as for a single ion. For example, for a magnetic dipole transition the matrix element is[39]

$$\langle E^1\mathbf{k} \mid \mathfrak{y} \mid G\rangle=[\Delta(\mathbf{k})/N]\sum_n \langle e_{n1} \mid \mathfrak{y}_{n1} \mid g_{n1}\rangle$$

$$=\Delta(\mathbf{k})\langle e_{01} \mid \mathfrak{y}_{01} \mid g_{01}\rangle, \qquad (4.11)$$

where $\mathfrak{y}_{01}$ is the single-ion magnetic dipole moment operator for the arbitrary site 01.

The response to external perturbations is the same as that calculated from a single-ion model. Consider, for example, an external magnetic field $H_0$ along the $z$ axis. The energy shift $\Delta W^\mu$ for excitons on sublattice $\mu$ is $\mathbf{k}$-independent and is given by

$$\Delta W^\mu=\beta H_0[\langle E^\mu\mathbf{k} \mid \sum_n L_{n\mu}{}^z+2S_{n\mu}{}^z \mid E^\mu\mathbf{k}\rangle]$$

$$=\beta H_0[g'\langle e_{0\mu} \mid S_{0\mu}{}^z \mid e_{0\mu}\rangle-g\langle g_{0\mu} \mid S_{0\mu}{}^z \mid g_{0\mu}\rangle]. \qquad (4.12)$$

This is equivalent to the result obtained in Sec. III.

The underlying reason why the pure electronic absorption can be described by a single-ion model is the fact that the excitation resides on a sublattice. When the excitations have no wave nature, it is immaterial whether the excitation resides on many equivalent ions or on one ion. This provides a sound theoretical basis for the single-ion description of these phenomena and presents guide lines for determining when single-ion descriptions are appropriate in other concentrated systems.

On the other hand, exciton effects are important for nonzero $\mathbf{k}$. Even though $V_{12}=0$, the exciton will have a $k$-dependent energy as long as $V_{11}$ does not also vanish. We have direct experimental evidence of this in our sideband data. The separation between lines $E1$ and $\sigma 1$ is 2.6 $cm^{-1}$ greater than the maximum magnon energy because the zone-boundary excitons have a greater energy than those at the zone center.

Considering only the first and third near neighbors (second neighbors are on opposite sublattice) in Eq. (4.9), the dispersion relation for excitons on either sublattice is

$$W(\mathbf{k})=W(E)+K_1\cos k_z c+K_3(\cos k_x a+\cos k_y a). \qquad (4.13)$$

From symmetry arguments similar to those presented in Sec. VI it can be shown that the $x$ and $y$ dispersion parameters must be the same. This also follows directly from group theory since the energy bands of a crystal must have the symmetry of the point group. Unfortunately, we cannot be sure that Eq. (4.13) adequately describes the exciton bands associated with $E1$ and $E2$, because the dispersion is rather sensitive to higher-order corrections resulting from the close proximity of the twelve levels of the ${}^4T_{1g}$ state. Including these corrections quickly makes the problem intractable, therefore, we accept Eq. (4.13) as a semiquantitative representation of the true dispersion.

## V. SPIN WAVES IN $MnF_2$

### A. Spin-Wave Dispersion

The antiferromagnetic properties of $MnF_2$ can be described by various approximations. For the temperatures of interest in these experiments ($T<\frac{1}{2}T_N$) the spin-wave approximation has been found to be extremely accurate. The theory has been discussed in great detail in the literature.[40,41] We shall only sketch it here for later reference and discuss those aspects which pertain directly to our optical studies.

We take as our Hamiltonian

$$\mathfrak{IC}=\mathfrak{IC}_e+\mathfrak{IC}_a+\mathfrak{IC}_z, \qquad (5.1)$$

[38] D. L. Dexter, J. Chem. Phys. **21**, 836 (1953).
[39] Define $\Delta(\mathbf{k}\neq 0)=0$ and $\Delta(\mathbf{k}=0)=1$.
[40] See for example, P. W. Anderson, Phys. Rev. **86**, 694 (1952); R. Kubo, Phys. Rev. **87**, 568 (1952); O. Nagai and A. Yoshimori, Progr. Theoret. Phys. (Kyoto) **25**, 595 (1961).
[41] J. Van Kranendonk and J. H. Van Vleck, Rev. Mod. Phys. **30**, 1 (1958).

where

$$\mathcal{H}_e = -J_1[\sum_{\langle i,i'\rangle} \mathbf{S}_i\cdot\mathbf{S}_{i'} + \sum_{\langle j,j'\rangle} \mathbf{S}_j\cdot\mathbf{S}_{j'}] - J_2\sum_{\langle i,j\rangle}\mathbf{S}_i\cdot\mathbf{S}_j,$$

$$\mathcal{H}_a = -(g\beta H_A)/2S[\sum_i (S_i{}^z)^2 + \sum_j (S_j{}^z)^2],$$

$$\mathcal{H}_z = g\beta H_0[\sum_i S_i{}^z + \sum_j S_j{}^z]. \quad (5.2)$$

Here $S$ is the spin of a manganese ion, and $i$ and $j$ refer to the spin-up (1) and spin-down (2) sublattices, respectively.

In the exchange term $\mathcal{H}_e$, we consider nearest-neighbor ($J_1$) and next-nearest-neighbor ($J_2$) exchange, and the sums are over the appropriate neighbor pairs. The anisotropy field $H_A$ phenomenologically represents the uniaxial anisotropy which in $MnF_2$ arises primarily from dipolar interactions.[42] The Zeeman energy for an external magnetic field $H_0$ along the $z$ axis is given by $\mathcal{H}_z$. The $g$ value is that appropriate for the ground state of the $Mn^{2+}$ ion in the concentrated system.

This Hamiltonian is now expressed in terms of the spin-wave normal modes. This is accomplished by first expressing the spin operator in terms of spin-deviation operators $a_i$ and $b_j$ satisfying boson commutation relations. Sublattice spin-wave operators $a_k$ and $b_k$ are then introduced by Fourier transforming the spin-deviation operators. Due to the exchange interaction these sublattice spin waves are coupled together. This coupling is diagonalized by transforming to new modes $\alpha_k$ and $\beta_k$. Retaining only quadratic terms, the Hamiltonian then becomes

$$\mathcal{H} = hc\sum_k [\nu_{1k}(\alpha_k{}^\dagger\alpha_k + \tfrac{1}{2}) + \nu_{2k}(\beta_k{}^\dagger\beta_k + \tfrac{1}{2})], \quad (5.3)$$

where the dispersion is given by

$$h c\nu_{1k,2k} = 2SZ_2\,|J_2|\,(1+0.073/2S) \times[(1+\epsilon_k)^2 - \gamma_k{}^2]^{1/2} \pm g\beta H_0 \quad (5.4)$$

with

$$\gamma_k = Z_2{}^{-1}\sum_\delta \exp(i\mathbf{k}\cdot\boldsymbol{\delta}) = \cos(\tfrac{1}{2}ak_x) \times \cos(\tfrac{1}{2}ak_y)\cos(\tfrac{1}{2}ck_z) \quad (5.5)$$

and

$$\epsilon_k = (g\beta H_A/2SZ_2\,|J_2|) - (2Z_1J_1/Z_2J_2)\sin^2\tfrac{1}{2}(k_z c). \quad (5.6)$$

Here $Z_1(=2)$ and $Z_2(=8)$ are the number of nearest- and next-nearest neighbors, respectively. The factor $(1+0.073/2S)$ takes account of the fact that even in the ground state there are small deviations from complete alignment.

### B. Magnetic Parameters in $MnF_2$

The magnetic parameters of $MnF_2$ have been measured by a variety of experiments. The Néel temperature is 67.34°K.[43] Magnetic susceptibility measurements by Trapp and Stout[44] combined with a low-temperature antiferromagnetic resonance measurement by Johnson and Nethercot[45] yield $H_A = 0.737$ cm$^{-1}$ (1.06°K) and $J_2 = -1.22$ cm$^{-1}$ (−1.76°K). Neutron-scattering experiments by Okazaki *et al.*,[46] when combined with the above values of $J_2$ and $H_A$, yield $J_1 = 0.22$ cm$^{-1}$ (0.32°K). Neutron scattering also puts an upper bound of 0.035 cm$^{-1}$ on the exchange coupling between nearest neighbors along the $x$ and $y$ axes ($J_3$). Thus, it is quite justifiable to neglect it. We note that the intersublattice exchange $J_2$, coupling the body-centered ion to the eight corner ions of the unit cell, is antiferromagnetic, whereas the intrasublattice exchange $J_1$, coupling the nearest neighbors along the $z$ axis, is ferromagnetic.

The spin-wave dispersion obtained by using these parameters in Eq. (5.4) is shown in Fig. 6. The two directions shown, **k** parallel to $z$ and **k** parallel to $x$, are the two extreme cases. All curves for other directions of **k** fall between these two.

### C. Spin-Wave Renormalization

The spin-wave theory described above is only appropriate for zero temperature. As the temperature increases from zero we must consider the quartic and higher-order terms in $\alpha_k$ and $\beta_k$ which appear in the Hamiltonian. These terms correspond to spin-wave scattering with the result that the energy of a given

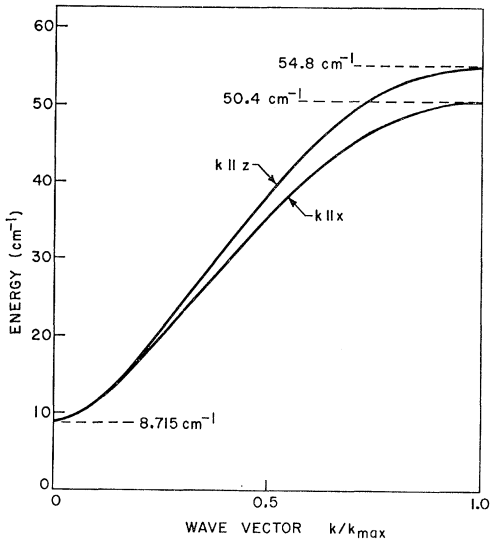


FIG. 6. Spin-wave dispersion in $MnF_2$ for the parameters $J_1 = 0.22$ cm$^{-1}$ (0.32°K), $J_2 = -1.22$ cm$^{-1}$ (−1.76°K), and $H_A = 0.737$ cm$^{-1}$ (1.06°K).

[42] F. Keffer, Phys. Rev. **87**, 608 (1952).

[43] P. Heller, Phys. Rev. **146**, 403 (1966).

[44] Charles Trapp and J. W. Stout, Phys. Rev. Letters **10**, 157 (1963).

[45] F. M. Johnson and A. H. Nethercot, Jr., Phys. Rev. **114**, 705 (1959).

[46] A. Okazaki, K. C. Turberfield, and R. W. H. Stevenson, Phys. Letters **8**, 9 (1964).

spin-wave mode depends upon the thermal occupation of the other modes. This can be described by defining a renormalization factor $R_k(T)$ such that the energy of a mode is

$$\nu_k(T) = R_k(T)\nu_k, \tag{5.7}$$

where $\nu_k$ is the energy for $T=0$.

Our optical data provides one of the most stringent experimental tests of renormalization in an antiferromagnet; thus, it is important to obtain accurate theoretical values for $R_k(T)$. A meaningful comparison can be made in $MnF_2$ since the magnetic parameters are well known. One of us[47] has calculated the renormalization in $MnF_2$ for several different spin-wave approximations. We shall review these results for later use in Sec. VII.

First of all, assume only intersublattice exchange $J_2$ (neglect $J_1$ and $H_A$). Expressing the spin operators in terms of the $\alpha_k$'s and $\beta_k$'s and carrying the expansion to fourth order, the diagonal terms in the Hamiltonian are

$$\mathcal{H}' = E_0 + 2\sum_k \nu_k n_k - 2(2Z_2J_2S^2N)^{-1}\sum_{kk'} \nu_k\nu_{k'} n_k n_{k'}. \tag{5.8}$$

Following Bloch,[48] the free energy is minimized with respect to $\langle n_k\rangle$. It is found that $\langle n_k\rangle$ has a boson thermal distribution with a renormalized energy $\nu_k(T)$ which depends upon temperature,

$$R(T) = \nu_k(T)/\nu_k = 1 - (Z_2J_2S^2N)^{-1}\sum_{k'} \nu_{k'}\langle n_{k'}\rangle. \tag{5.9}$$

This says that the spin-wave energies are renormalized by the total-spin-wave energy. Since $\langle n_{k'}\rangle$ depends upon $\nu_{k'}(T)$ this is an implicit equation. We note that in this approximation the renormalization factor is independent of $\mathbf{k}$. It is not valid to transform the sum to an integral and extend the integral to infinity for this overestimates the spin-wave energy. Therefore, the sum is evaluated numerically to appropriately take account of Brillouin-zone effects. The result of this calculation is indicated by the curve marked $R^1$ in Fig. 7.

Low[49] has carried out the procedure outlined above including $J_1$, $J_2$, and $H_A$. He finds

$$R_k(T) = 1 - (\alpha_k/NS)\sum_{k'} \alpha_{k'}[(1+\epsilon_{k'})^2 - \gamma_{k'}^2]^{1/2}\langle n_{k'}\rangle, \tag{5.10}$$

where

$$\alpha_k = (1+\epsilon_k-\gamma_k^2)/[(1+\epsilon_k)^2-\gamma_k^2], \tag{5.11}$$

and $\gamma_k$ and $\epsilon_k$ are defined above in Eqs. (5.5) and (5.6). From Eq. (5.4) we see that the quantity within the square bracket is the zero-temperature spin-wave energy. Thus, except for the factor $\alpha_k$, Eq. (5.10) has the same form as Eq. (5.9). In this case the renormalization factor depends upon $\mathbf{k}$. Equation (5.10) has been evaluated for spin waves at $X(k_x=\pi/a,\ k_y=k_z=0)$ and $Z(k_x=k_y=0,\ k_z=\pi/c)$. The results are indicated by $R_x^2$ and $R_z^2$, respectively, in Fig. 7.

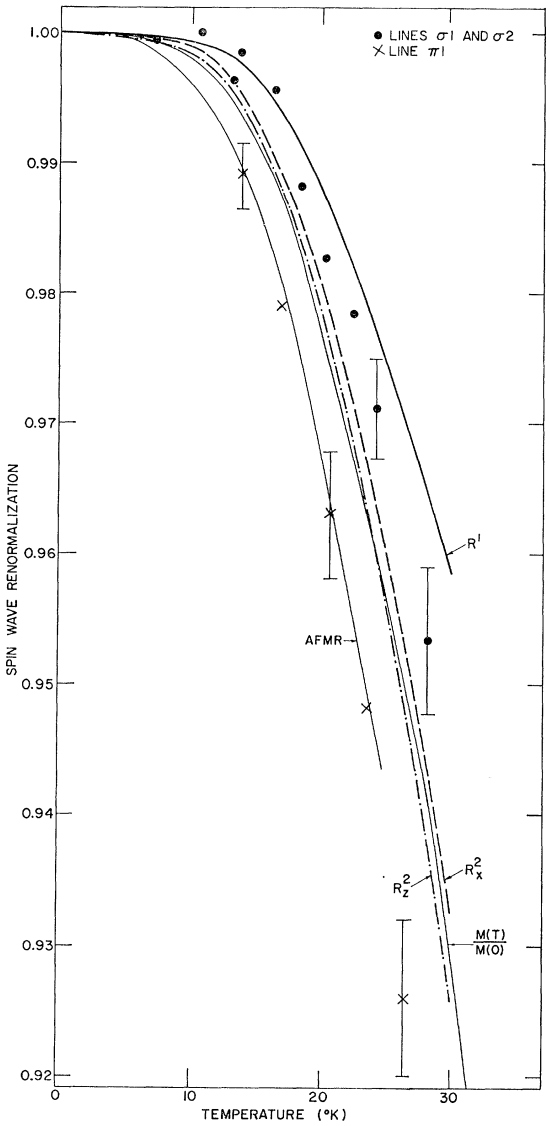


FIG. 7. The observed and calculated renormalization factors for $MnF_2$. The optical data are plotted as solid circles for lines $\sigma 1$ and $\sigma 2$ and as $X$'s for line $\pi 1$. The antiferromagnetic resonance (AFMR) and sublattice magnetization $M(T)/M(O)$ data are also shown. The theoretical curves are denoted by $R^1$, $R_x^2$,and $R_z^2$. For $R^1$ only $J_2$ is considered. For $R_x^2(\mathbf{k}=\hat{x}\pi/a)$ and $R_z^2(\mathbf{k}=\hat{z}\pi/c)$, $J_1$, $J_2$, and $H_A$ are included.

We note that all the $R(T)$ fall reasonably close to the normalized sublattice magnetization $M(T)/M(0)$ for the temperatures considered ($T<30$°K). It is an interesting question whether there is a good physical or theoretical reason for this or whether this is merely an accident. The sublattice magnetization for an antiferromagnet is given by (if zero-point deviations are

[47] R. M. White, Phys. Letters **19**, 453 (1965).
[48] Micheline Bloch, Phys. Rev. Letters **9**, 286 (1962).
[49] G. G. Low, *Inelastic Scattering of Neutrons* (International Atomic Energy Agency, Vienna, 1965), p. 453.

neglected)

$$[M(T)/M(0)]=1-(NS)^{-1}\sum_{\mathbf{k}'}(1+2v_{\mathbf{k}'}^2)\langle n_{\mathbf{k}'}\rangle. \quad (5.12)$$

In a ferromagnet the situation is simpler since the $v_{\mathbf{k}}^2$ term is absent. In that case we find that $R(T)$ equals $M(T)/M(0)$ if we assume an "Einstein" spin-wave spectrum with half the maximum spin-wave energy, $ZJS$. For the antiferromagnet we cannot make such a simple correspondence, but nevertheless, we see that the forms of Eqs. (5.9) and (5.12) are similar and furthermore the differences tend to be averaged out by the sum over $\mathbf{k}$.

### D. Exciton Nature of Spin Waves

For this problem in which we deal with both spin waves and excitons, it is important to emphasize the exciton nature of a spin wave. One way of illustrating this similarity is to show that the usual expression for a spin wave can be cast into the form used in Sec. IV.A to describe excitons. In the usual theory a spin wave with wave vector $\mathbf{k}$ is that state formed when the creation operator $a_{\mathbf{k}}^\dagger$ acts upon the vacuum state $|\,\mathrm{vac}\rangle$ We can transform from occupation space to ordinary space by noting that $a_{\mathbf{k}}^\dagger$ is the Fourier transform of $a_{n1}^\dagger$ which in turn is proportional to $S_{n1}^-$. If we assume that the ground state is that of complete alignment[50,51] then the sublattice magnon is given by

$$|M^1\mathbf{k}\rangle=a_{\mathbf{k}}^\dagger\,|\,\mathrm{vac}\rangle=N^{-1/2}\sum_n \exp(i\mathbf{k}\cdot\mathbf{r}_{n1})\,|\,M_{n1}\rangle, \quad (5.13)$$

where

$$|\,M_{n1}\rangle=S_{n1}^-\,|\,G\rangle. \quad (5.14)$$

That is, a spin wave is a phased linear superposition of states in which one ion is excited from its aligned state $|\,g\rangle$ with $M_s=S$ to the ("tipped") state $|\,m\rangle=S^-\,|\,g\rangle$ with $M_s=\mathrm{S}-1$. We see immediately that a spin wave is an exciton formed from the spin-degenerate ground state of the ion. Thus, it is not surprising that two-magnon and exciton-magnon absorption have similar characteristics (since both are two-exciton processes).

## VI. THEORY OF EXCITON-MAGNON INTERACTIONS

In general, exciton-magnon interactions can lead to transitions and energy shifts. We are primarily interested in transitions corresponding to exciton-magnon absorption. We find that this interaction is quite small, and that we have a situation in which the coupling is strong enough to cause observable transitions yet not sufficiently strong to appreciably distort the energies.

It will be seen that the interaction involving an exciton and a magnon can be described in terms of the interactions of pairs of ions even though the excitons and magnons are spread throughout the laittce. Being nonlocal excitations, however, the total interaction is a (phased) linear combination of all pair interactions.

We can represent exciton-magnon absorption by the simple diagram in Fig. 8. Initially, both ions are in the ground state and a photon is present. The photon is absorbed and finally, the ions are excited to states $|\,e\rangle$ and $|\,m\rangle$, respectively. For two-magnon absorption both ions are excited to the $|\,m\rangle$ states. It is quite obvious that these are closely related phenomena. The basic questions for such transitions are the following: (1) What mechanism can couple the transitions of neighboring ions so that both are excited by a single photon? (2) How can such transitions be electric-dipole processes when both single-ion transitions are parity forbidden?

In early discussions of exciton-magnon absorption two seemingly dissimilar mechanisms were suggested by Halley and Silvera[9] and by Tanabe, Moriya, and Sugano.[19] Allen, Loudon, and Richards[10] first pointed out that these two mechanisms are quite similar and that they are both special cases of an earlier theory proposed by Dexter[20] to explain electric-dipole absorption by pairs of ions, which is clearly a closely related problem.

Dexter used the Coulomb interaction to couple the ions. As we have seen in our discussion of excitons this leads to direct and exchange terms. Halley and Silvera used the direct term together with spin-orbit coupling but ignored the exchange term. Tanabe, Moriya, and Sugano pointed out the importance of the latter.

In this section we describe the exciton-magnon interaction using the formalism of Sec. IV. We consider the characteristics for both the direct and exchange Coulomb interaction and discuss the relative importance of these mechanisms.

### A. Form of the Interaction

The Hamiltonian of a crystal including the electric-dipole perturbation of an optical electric field $\boldsymbol{\mathcal{E}}$ can be written as

$$\mathcal{H}=\mathcal{H}_0+V+\boldsymbol{\mathcal{E}}\cdot\mathbf{P}, \quad (6.1)$$

where $\mathbf{P}$ is the sum of the electric-dipole operators of

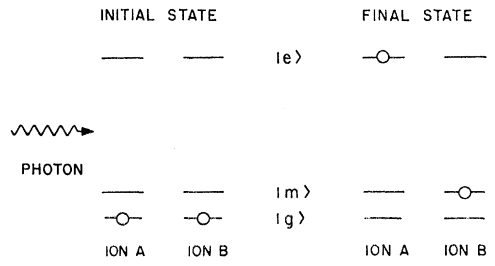


FIG. 8. Schematic representation of exciton-magnon absorption in terms of the transitions of a pair of ions.

[50] This approximation is discussed in Ref. 41. These authors have shown that even in the worst case when $H_A\to 0$, this approximation is 93% correct.

[51] E. D. Jones and K. B. Jefferts, Phys. Rev. **135**, A1277 (1964). These authors have measured the zero-point deviation in $MnF_2$ and have found it to be less than 1%.

all electrons, $H_0$ is the sum of all single-ion Hamiltonians, and $V$ is the total-interion Coulomb interaction. The eigenstates of $\mathcal{H}_0+V$, obtained in the Sec. IV, form the basis for perturbation theory. We remember, however, that these are not exact eigenstates since the matrix elements of $V$ between nondegenerate ionic states were neglected. These terms are essential here for, in addition to the electric dipole term, they constitute the perturbation which leads to exciton-magnon absorption.

In first order this perturbation does not lead to the desired transition. This is easily seen since $\mathbf{P}$ can only connect states differing by one excitation. The $V$ and $\mathbf{P}$ perturbations must be combined in second order to form an effective Hamiltonian which connects the ground state $|G\rangle$ with the final exciton-magnon (or two magnon) state $|F\rangle$. Consequently, the interaction has the form

$$\langle F|\mathcal{H}^{\text{eff}}|G\rangle=\sum_u \boldsymbol{\varepsilon}\cdot\left[\frac{\langle F|V|U\rangle\langle U|\mathbf{P}|G\rangle}{W(G)-W(U)+h\nu}+\frac{\langle F|\mathbf{P}|U'\rangle\langle U'|V|G\rangle}{W(G)-W(U')}\right], \quad (6.2)$$

where the sum is over all intermediate states. The energies of the ground and intermediate states of the crystal are $W(G)$ and $W(U)$, respectively, and the wave number of the photon absorbed is $\nu$. This is the basic expression for our discussion of the exciton-magnon interaction. From it, with the aid of crystal symmetry, we obtain a detailed description of the observed transitions.

Several characteristics of the interaction can be determined from the form of Eq. (6.2). For centrosymmetric crystals and $3d$-electronic states the initial and final states have even parity. As a result of this and the fact that $V$ is a two-electron scalar operator and $\mathbf{P}$ is a one-electron vector operator, $|U\rangle$ must be an odd-parity exciton state and $|U'\rangle$ must be a state with one magnon and one odd-parity exciton. The odd-parity exciton is formed from odd-parity single-ion transitions such as those obtained by promoting one $3d$ electron to a $p$ state. These odd states are high-lying states; therefore, the energy denominators are typically on the order of $10^5$ cm$^{-1}$.

A second property of the interaction follows from the conservation of quasimomentum in a periodic system. Since the ground state has no quasimomentum, the sum of the $\mathbf{k}$ vectors for the two final excitations must vanish. Thus, for example, we have

$$\langle U|\mathbf{P}|I\rangle=\Delta(\mathbf{k}'')\langle u_{01}|\mathbf{P}_{01}|g_{01}\rangle \quad (6.3)$$

and

$$\langle F|V|U\rangle=\Delta(\mathbf{k}+\mathbf{k}'-\mathbf{k}'')\sum_n \exp(i\mathbf{k}\cdot\boldsymbol{\delta}_{01,n2})\times\langle e_{01}m_{n2}|V_{01,n2}|\mathcal{P}u_{01}g_{n2}\rangle, \quad (6.4)$$

where $\mathbf{P}_{01}$ is the sum of the dipole operators of the electrons at site 01, and $\boldsymbol{\delta}_{01,n2}$ is a vector from site 01 to site $n2$.

The matrix elements in these expressions include both spatial integrations and spin sums. Since $V$ and $\mathbf{P}$ do not operate in spin space, the spin sums lead directly to several interesting results. Initially, let us ignore spin-orbit coupling to the ground state. Then $|g_{01}\rangle$ has $M_s=\frac{5}{2}$, $|g_{n2}\rangle$ has $M_s=-\frac{5}{2}$, and $|m_{n2}\rangle$ has $M_s=-\frac{3}{2}$. Equation (6.3) requires that $\langle u_{01}|$ have $M_s=\frac{5}{2}$. It is then clear that the *direct* term in Eq. (6.4) must vanish due to the fact that $|g_{n2}\rangle$ and $|m_{n2}\rangle$ have different $M_s$ values. The *exchange* terms, on the other hand, can contribute provided $|e_{01}\rangle$ has $M_s=\frac{3}{2}$. Thus, we find that the absorption matrix element is nonvanishing only if there is an electron exchange between opposite sublattices. Notice that neither the direct nor the exchange terms can contribute if both ions are on the same sublattice.

If spin-orbit coupling to the ground state is included, the direct terms can contribute. In the matrix elements in Eq. (6.4), for example, spin orthogonality can be satisfied by two orders of spin-orbit coupling to the ground state at site $n2$ and one order of coupling in the odd states at site 01. We expand the Coulomb interaction in multipole moments and find that the lowest-order term is the interaction of the quadrupole moment at site $n2$ with the dipole moment at 01. In contrast with the exchange terms, this interaction contributes when the two ions are on the same sublattice as well as on opposite sublattices.

Since the direct and exchange interactions have quite similar characteristics it is different to differentiate between them experimentally. There is some evidence, however, that the exchange interaction predominates in $MnF_2$. First of all, it is observed that two-magnon absorption in $MnF_2$ and $FeF_2$ has comparable strength. If this absorption results from the direct interaction, it should be approximately four orders of magnitude weaker in $MnF_2$ because of the smaller spin-orbit coupling to the ground state.[10] Further evidence is provided by the magnetic-field behavior of exciton-magnon absorption in $MnF_2$. The lines do not split or shift in a magnetic field thus indicating, as we shall see, that the excitons and magnon are on opposite sublattices.[51a] This is in accord with the predictions of the exchange interaction. But since the direct interaction permits intrasublattice coupling, we expect that it would lead to lines that would split or broaden in a magnetic field.

We conclude that the exchange interaction is more important in $MnF_2$. If there is a direct quadrupole-dipole interaction, the resulting intrasublattice coupling is unobservable in $MnF_2$. Thus, we concentrate upon intersublattice coupling.

Gondaira and Tanabe[36] have considered an additional mechanism involving polar intermediate states which are not included in this formalism. We shall not discuss

[51a] See note added in proof.

their mechanism since we are primarily motivated to describe the observed lines in $MnF_2$, and the interactions discussed here provide an adequate basis for this.

If we restrict our attention to the case with interactions between sublattices, there are two possible final states (for each $\mathbf{k}$), $|E^1\mathbf{k};M^2-\mathbf{k}\rangle$ and $|E^2\mathbf{k};M^1-\mathbf{k}\rangle$. These are eigenstates for the exciton, but for a general $\mathbf{k}$ they are not eigenstates for the magnon. For the final state $|E^1\mathbf{k};M^2-\mathbf{k}\rangle$, the complete expression for Eq. (6.2) in terms of single-ion matrix elements is given by

$$\langle E^1\mathbf{k};M^2-\mathbf{k}|\mathcal{H}^{\text{eff}}|G\rangle=\sum_{n=1}^{N}\exp(i\mathbf{k}\cdot\boldsymbol{\delta}_{01,n2})\,\mathcal{E}$$
$$\times\Big[\sum_u\Big\{\frac{\langle e_{01}m_{n2}|V_{01,n2}|\mathcal{P}u_{01}g_{n2}\rangle\langle u_{01}|\mathbf{P}_{01}|g_{01}\rangle+\langle e_{01}m_{n2}|V_{01,n2}|\mathcal{P}g_{01}u_{n2}\rangle\langle u_{n2}|\mathbf{P}_{n2}|g_{n2}\rangle}{W(G)-W(U)+hc\nu}$$
$$+\frac{\langle e_{01}|\mathbf{P}_{01}|u_{01}\rangle\langle u_{01}m_{n2}|V_{01,n2}|\mathcal{P}g_{01}g_{n2}\rangle+\langle m_{n2}|\mathbf{P}_{n2}|u_{n2}\rangle\langle e_{01}u_{n2}|V_{01,n2}|\mathcal{P}g_{01}g_{n2}\rangle}{W(G)-W(U)}\Big\}\Big]. \quad (6.5)$$

This result supports our assertion that the interaction can be described in terms of pair interactions. The expression within the square brackets describes the process shown in Fig. 8. It is the effective transition electric-dipole moment of the pair of ions 01 and $n2$. This expression is equivalent to Dexter's[20] Eq. (5). The total moment is the sum of pair moments,

$$\langle E^1\mathbf{k};M^2-\mathbf{k}|\mathcal{H}^{\text{eff}}|G\rangle=\sum_{n=1}^{N}\exp(i\mathbf{k}\cdot\boldsymbol{\delta}_{01,n2})\,\mathcal{E}$$
$$\times\langle e_{01}m_{n2}|\mathbf{P}_{01,n2}{}^{\text{eff}}|\mathcal{P}g_{01}g_{n2}\rangle, \quad (6.6)$$

in which each term is multiplied by a phase factor which accounts for the orientation of the pair. The sum extends over all sites on sublattice 2. Since $\mathbf{P}_{01,n2}{}^{\text{eff}}$ depends upon the overlap of the wave functions it is a rapidly decreasing function of distance; therefore, it is justifiable to truncate the sum to the neighboring ions. The first and third nearest neighbors are automatically excluded because they are on the same sublattice. For the discussion of symmetry in the following section we consider the eight second-nearest neighbors.

### B. Symmetry and Selection Rules

In this section we shall simplify Eq. (6.6) by using the symmetry of the $MnF_2$ crystal.[52] The symmetry operations appropriate to $MnF_2$ are listed in Appendix A. Let us begin by labeling the ions as shown in Fig. 3 and defining the following quantities. If the exciton is on sublattice 1, we represent the $j$th component of the matrix element of $\mathbf{P}^{\text{eff}}$ for the pair of ions $0$–$n$ by $P_n{}^j$. If the exciton is on sublattice 2, we denote this by $Q_n{}^j$. Also, we denote the $j$th component of the total-effective-transition electric-dipole moment by $M_1{}^j$ and $M_2{}^j$ for the respective cases. Then substituting explicitly for $\boldsymbol{\delta}_{01,n2}$ and restricting the sum to the eight second-nearest neighbors, Eq. (6.6) becomes

$$M_1{}^j(\mathbf{k})=\exp(ik_zc/2)\{P_1{}^j\exp[i(k_x-k_y)a/2]+P_2{}^j\exp[i(k_x+k_y)a/2]+P_3{}^j\exp[i(-k_x+k_y)a/2]$$
$$+P_4{}^j\exp[i(-k_x-k_y)a/2]\}+\exp(-ik_zc/2)$$
$$\times\{P_5{}^j\exp[i(k_x-k_y)a/2]+P_6{}^j\exp[i(k_x+k_y)a/2]+P_7{}^j\exp[i(-k_x+k_y)a/2]+P_8{}^j\exp[i(-k_x-k_y)a/2]\}, \quad (6.7)$$

for the case with the exciton on sublattice 1.

We begin by considering the four elements $(E\,|\,0)$; $(C_2{}^z\,|\,0)$; $(I\,|\,0)$ and $(\sigma_h\,|\,0)$ which form the unitary site group for rutile in the magnetically ordered state. In particular, consider the symmetry operation $(C_2{}^z\,|\,0)$. This is a pure rotation by $\pi$ about a $z$ axis through the site 0. For the ions which do not lie on the rotational axis the transformation consists of two steps: (1) Translate the ion to a new site; (2) rotate the contours of the wave function.

It is clear that the matrix element $P_3{}^z$ of the original crystal, for example, is related to $P_1{}^z)_T$ of the transformed crystal. We obtain the relationship between $P_3{}^z$ and $P_1{}^z)_T$ from the transformation properties of the functions within the matrix element $\langle e_{01}m_{n2}|(\mathbf{P}^{\text{eff}})_z|g_{01}g_{n2}\rangle$. The dipole operator $\mathbf{P}^{\text{eff}}$ transforms like a polar vector, thus under a rotation about the $z$ axis the $z$ component goes into itself. The effect of the transformation upon the wave functions is found by applying the usual theory of rotation properties of angular momentum functions. For the special case of rotations about the quantization axis we have

$$R(\theta_z)\,|JM\rangle=\exp(iM\theta_z)\,|JM\rangle. \quad (6.8)$$

For the sidebands we are considering, the state $|e\rangle$

[52] Further details are given by D. D. Sell, Ph.D. thesis, Stanford University, Stanford, California, 1967 (unpublished).

has $S=\frac{3}{2}$, $M_s=\frac{3}{2}(-\frac{3}{2})$ for the spin-up (-down) sublattice. Orbitally, $|e\rangle$ is a linear combination of the $\pm 1$ components of $T_{1g}$. In Sec. IV we found that these components of $T_{1g}$ are formed from the odd-$M_L$ components of $P$, $F$, and $G$ free-ion states. Using Eq. (6.8) with $\theta=\pi$ we find that

$$|g_0\rangle\langle e_0| \rightarrow |g_0\rangle\langle e_0|,$$
$$|g_3\rangle\langle m_3| \rightarrow -|g_1\rangle\langle m_1|. \tag{6.9}$$

We use this notation for a product of wave functions to differentiate it from a matrix element which is written as $\langle e|g\rangle$. In Sec. VI.C we show how the transformation properties of such products can be obtained group theoretically. Combining this with the transformation of $P^{\text{eff}})_z$ we find that $P_3{}^z \rightarrow -P_1{}^z)_T$. Since the transformed crystal is identical with the original one, we require that $P_1{}^z)_T=P_1{}^z$ and conclude that $P_3{}^z=-P_1{}^z$.

In a similar manner we can apply the other three symmetry operations to the $P_n{}^j$ and obtain all possible relationships between these quantities. Equation (6.7) then reduces to

$$M_1{}^z(\mathbf{k})=4i\cos(k_zc/2)[P_1{}^z\sin(k_x-k_y)a/2+P_2{}^z\sin(k_x+k_y)a/2],$$
$$M_1{}^{\xi,\eta}(\mathbf{k})=4i\sin(k_zc/2)[P_1{}^{\xi,\eta}\cos(k_x-k_y)a/2+P_2{}^{\xi,\eta}\cos(k_x+k_y)a/2]. \tag{6.10}$$

No further information is obtained from the other four unitary elements (5–8 in Appendix A).

The results for the case with the exciton on sublattice 2 are obtained by using $(C_2{}^z|\tau)$. We find that the roles of $\xi$ and $\eta$ are simply interchanged; thus, for example, $P_1{}^\xi \rightarrow -iQ_2{}^\eta$.

The absorption coefficient for exciton-magnon absorption is proportional to $|M|^2$. In Sec. VII we shall use Eq. (6.10) to obtain calculated shapes and polarizations of the absorption lines. It is important to note that Eq. (6.10) is rather general since it depends primarily upon symmetry. The details of the wave functions and the interaction mechanism are isolated in the three matrix elements which can be considered phenomenological parameters.

We can obtain the transition moment for other final states in a similar way. For two-magnon absorption when the magnons are on opposite sublattices we obtain the results of Allen, Loudon, and Richards.[10] For exciton-magnon and two-magnon absorption when both excitations are on the same sublattice, the weighting factors suppress all critical points. Furthermore, in the two-magnon case translational symmetry requires the moment to vanish.

### C. Exciton and Magnon Symmetries

In the previous subsection we showed how a detailed knowledge of the transformation properties of $|g\rangle$, $|m\rangle$, and $|e\rangle$ led to selection rules for various processes involving excitons and magnons. In this subsection we shall rederive these results by considering the symmetry of the excitons and magnons themselves. While the first approach is more physically transparent, this second approach enables us to use all the powerful tools of group theory, thereby obtaining a more general result.

We begin by finding the irreducible representations for the excitons and magnons. Dimmock and Wheeler[53] have given the irreducible representations of the (unitary) group of $\mathbf{k}$ for all the symmetry points and lines in the Brillouin zone of $MnF_2$, as well as the compatibility relations between these representations. Let us begin by considering the point $\Gamma$. The character table for $\Gamma$ is shown in Table II. We also indicate the transformation properties of the components of a pseudovector $(S_x, S_y, S_z)$ and a polar vector $(x, y, z)$. It is easily seen that this group is isomorphic to the point group group $D_{2h}$ (which is obtained by setting $\tau$

TABLE II. Character table for the point $\Gamma$ of the space group $P_{nnm}$ or $D_{2h}$[12]. The transformation properties of a pseudovector $(S_x,S_y,S_z)$ and a polar vector $(x,y,z)$ are indicated. Under time-reversal symmetry, $\Gamma_3{}^+$, $\Gamma_4{}^+$ and also $\Gamma_3{}^-$, $\Gamma_4{}^-$ become degenerate.

| | $\Gamma_1{}^+$ | $\Gamma_2{}^+$ $S_z$ | $\Gamma_3{}^+$ $S_x$ | $\Gamma_4{}^+$ $S_y$ | $\Gamma_1{}^-$ | $\Gamma_2{}^-$ $z$ | $\Gamma_3{}^-$ $x$ | $\Gamma_4{}^-$ $y$ | $\Gamma_5{}^+$ | $\Gamma_5{}^-$ |
|---|---|---|---|---|---|---|---|---|---|---|
| $(E\|0)$ | 1 | 1 | 1 | 1 | 1 | 1 | 1 | 1 | 2 | 2 |
| $(\bar{E}\|0)$ | 1 | 1 | 1 | 1 | 1 | 1 | 1 | 1 | −2 | −2 |
| $(C_2{}^z,\bar{C}_2{}^z\|0)$ | 1 | 1 | −1 | −1 | 1 | 1 | −1 | −1 | 0 | 0 |
| $(C_2{}^x,\bar{C}_2{}^x\|\tau)$ | 1 | −1 | 1 | −1 | 1 | −1 | 1 | −1 | 0 | 0 |
| $(C_2{}^y,\bar{C}_2{}^y\|\tau)$ | 1 | −1 | −1 | 1 | 1 | −1 | −1 | 1 | 0 | 0 |
| $(I\|0)$ | 1 | 1 | 1 | 1 | −1 | −1 | −1 | −1 | 2 | −2 |
| $(\bar{I}\|0)$ | 1 | 1 | 1 | 1 | −1 | −1 | −1 | −1 | −2 | 2 |
| $(\sigma_h,\bar{\sigma}_h\|0)$ | 1 | 1 | −1 | −1 | −1 | −1 | 1 | 1 | 0 | 0 |
| $(\sigma_{vx},\sigma_{vx}\|\tau)$ | 1 | −1 | 1 | −1 | −1 | 1 | −1 | 1 | 0 | 0 |
| $(\sigma_{vy},\sigma_{vy}\|\tau)$ | 1 | −1 | −1 | 1 | −1 | 1 | 1 | −1 | 0 | 0 |

[53] J. O. Dimmock and R. G. Wheeler, Phys. Rev. **127**, 391 (1962).

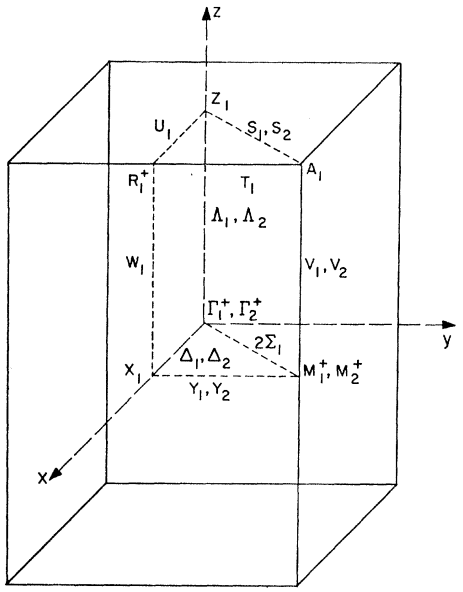


FIG. 9. Irreducible representations for the excitons for the symmetry points and planes of the Brillouin zone (after R. Loudon, Ref. 54).

equal to zero). In the full group including time reversal the pairs of representations $\Gamma_3^+$, $\Gamma_4^+$ and $\Gamma_3^-$, $\Gamma_4^-$ become degenerate.

The sublattice magnon for $\mathbf{k}=0$ is

$$|M^1, \mathbf{k}=0\rangle = N^{-1/2}\sum_n S_{n1}^- |G\rangle. \quad (6.11)$$

The ground state $|G\rangle$ must transform as $\Gamma_1^+$ for, by definition, it is invariant under all group operations. Consequently, for sublattice 1 the magnon transforms as $S^-$ which we see transforms as $\Gamma_3^+$, $\Gamma_4^+$. Similarly, for sublattice 2, $|M^2, \mathbf{k}=0\rangle$ transforms as $S^+$ which also belongs to $\Gamma_3^+$ and $\Gamma_4^+$. Neither sublattice magnon transforms as a single irredicible representation but this is not inconsistent. First of all, the true eigenstates are linear combinations of these states. Secondly, $\Gamma_3^+$ and $\Gamma_4^+$ become degenerate in the full space group. Symmetry tells us that at $\Gamma$ the two magnon modes must be degenerate (i.e., no Davydov splitting).

The transformation properties of the excitons can be obtained from the polarizations of lines $E1$ and $E2$. These are magnetic dipole lines appearing in $\sigma$ (electric) polarizations, thus the transition matrix element is

$$\langle E, \mathbf{k}=0 | \mu^z | G\rangle. \quad (6.12)$$

Since $\mu^z$ transforms as $\Gamma_2^+$, the exciton must also transform as $\Gamma_2^+$.

Now we can easily obtain the transformation properties of $|g\rangle\langle e|$ and $|g\rangle\langle m|$ which we used in subsection B. We note that an exciton state can be written as

$$|E^1\mathbf{k}\rangle = [N^{-1/2}\sum_n \exp(i\mathbf{k}\cdot\mathbf{r}_{n1})\, |e_{n1}\rangle\langle g_{n1}|]\,|G\rangle. \quad (6.13)$$

Loudon[54] refers to $|e\rangle\langle g|$ as the transition operator. For $\mathbf{k}=0$, the sublattice exciton transforms like $|^1e\rangle\langle g|$, thus $|e\rangle\langle g|$ transforms as $S^z$. In a similar way we see from Eq. (6.11) that $|m\rangle\langle g|$ transforms as $S^-$ for sublattice 1 and as $S^+$ for sublattice 2.

We must note that our discussion of exciton symmetry is somewhat oversimplified. Loudon[54] has shown that the two excitons resulting from this single-ion transition must transform as $\Gamma_1^+$ and $\Gamma_2^+$, respectively. We can see this by returning to Eq. (4.10). The state $|E^+, \mathbf{k}=0\rangle$ transforms as $\Gamma_2^+$ and $|E^-, \mathbf{k}=0\rangle$ transforms as $\Gamma_1^+$. Unlike the magnons, time-reversal symmetry does not require these states to be degenerate, thus, in general, Davydov splitting may occur. In $MnF_2$, however, they are degenerate, and we are free to choose sublattice excitons as eigenstates. Incidentally, we note that Davydov splitting (if it exists) can not be observed in an unperturbed crystal because $\Gamma_1^+$ does not transform as a vector component. This is verified by our model. The contributions to the transition moment from the two sublattices cancel for $|E^-, \mathbf{k}=0\rangle$.

The irreducible representations of the excitons and magnons for the symmetry lines and points of the Brillouin zone can be obtained as follows by using the compatibility and character tables of Dimmock and Wheeler[53]: (1) For the symmetry points, the representations are obtained by comparing the characters for the respective groups of $\mathbf{k}$ with those for $\Gamma$ for the elements $(R\,|\,0)$ common to both. (2) For the symmetry lines, the compatibility tables can be used. The

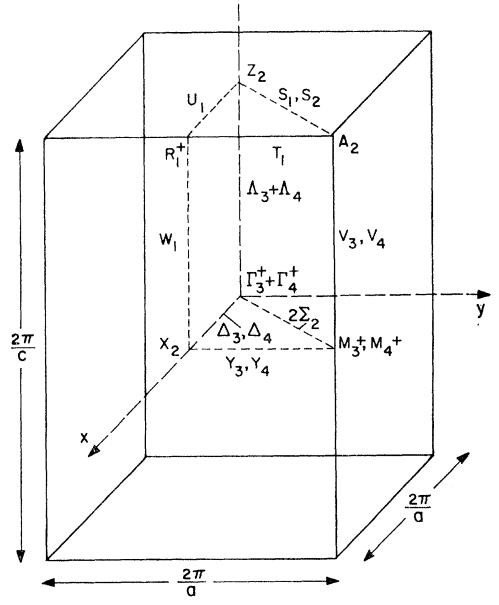


FIG. 10. Irreducible representations for the magnons. The notation $\Gamma_3^+ + \Gamma_4^+$ denotes that these representations are degenerate because of time-reversal (after R. Loudon, Ref. 54).

[54] R. Loudon (to be published).

results for the excitons and magnons are shown in Figs. 9 and 10, respectively.

The selection rules for exciton-magnon absorption are determined by the transition matrix element

$$\langle E\mathbf{k}; M-\mathbf{k} \mid \mathbf{P} \mid G\rangle. \tag{6.14}$$

Lax and Hopfield[55] have discussed a method for obtaining selection rules connecting different points in $\mathbf{k}$ space which uses the available character tables for the groups of $\mathbf{k}$. We are primarily interested in the symmetry points at the zone boundary since these lead to critical points in the density of states. As we have shown in Ref. 11, the sideband absorption is proportional to a weighted density of states. If the selection rules forbid the transition for some symmetry point, this peak in the density of states is suppressed by the weighting factor and does not appear in the observed spectrum. Using the method of Lax and Hopfield we find that the product representations for the exciton-magnon states at the symmetry points decompose into (note that the characters for $-\mathbf{k}$ are the complex conjugates of those of $\mathbf{k}$)

$$\begin{aligned} X_1\times X_2&=\Gamma_3^+ +\Gamma_4^+ +\Gamma_1^- +\Gamma_2^-,\\ M_1^+\times M_3^+&=M_2^+\times M_4^+=\Gamma_3^+,\\ M_1^+\times M_4^+&=M_2^+\times M_3^+=\Gamma_4^+,\\ Z_1\times Z_2&=A_1\times A_2=\Gamma_3^+ +\Gamma_4^+ +\Gamma_3^- +\Gamma_4^-,\\ R_1^+\times R_2^+&=\Gamma_1^+ +\Gamma_2^+ +\Gamma_3^+ +\Gamma_4^+. \end{aligned} \tag{6.15}$$

This provides the information necessary to determine the selection rules for any operator transforming as a $\Gamma$ representation. For the electric-dipole process we see that $X$ contributes to $\pi$ polarization and $Z$ and $A$ contribute to $\sigma$ polarization. For the two-magnon process, on the other hand, $Z$ contributes to $\pi$ polarization and $X$ contributes to $\sigma$ polarization. Since in this latter case we are dealing with two identical excitations the symmetrized Kronecker squares must be used rather than the usual Kronecker products. This causes the greater selectivity of the two-magnon process. For example, if a process involved a magnon and an exciton which transforms like the magnon, both $Z$ and $A$ could contribute to $\pi$ polarization.

We note that $M$ and $R$ do not contribute to either polarization. This is true because the groups at $M$ and $R$ contain inversion and the exciton and magnon states have even parity. Such a product state cannot decompose into odd-parity representations.

These selection rules are considerably more general than those obtained in the previous subsection. These results do not depend upon the nature of the interaction and make no assumptions restricting the excitons or magnons to a given sublattice. The selection rules follow solely from the fact that the excitons and magnons transform according to the irreducible representations of the groups of $\mathbf{k}$ as shown in Figs. 9 and 10.

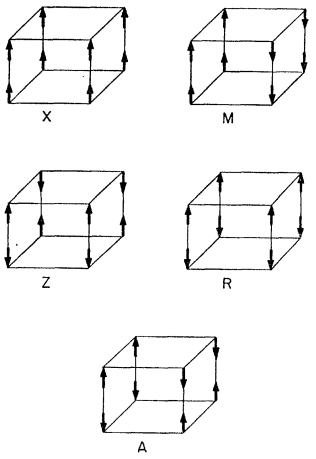


FIG. 11. The $z$ components of the pair transition moments of exciton-magnon absorption for the symmetry points in the Brillouin zone. Only the $X$ point can give a nonvanishing contribution.

It is clear that any proposed mechanism for this process must predict selection rules consistent with those obtained here, and indeed the results obtained in the previous subsection are consistent. From Eq. (6.10) we see that $X$ contributes to $\pi$ polarization ($M_1^z$) and $Z$ and $A$ contribute to $\sigma$ polarization ($M_1^\xi$, $M_1^\eta$) for coupling between sublattices.

In Fig. 11 we illustrate the $z$ components of the pair transition moments for the various symmetry points in the Brillouin zone. The arrow represents the moment for the ion at that site and the body-centered ion. The orientations of the vectors are determined by symmetry relations obtained as indicated in the previous subsection and by the phase factor $\exp(i\mathbf{k}\cdot\boldsymbol{\delta})$ for the various values of $\mathbf{k}$. A macroscopic electric field "sees" the sum of these pair moments. It is clear that the dipole moments sum to zero for all symmetry points except $X$ and that there is inversion symmetry for the points $M$ and $R$.

## VII. DISCUSSION

In this section we shall apply the theory of the preceding sections to analyze the sidebands.

### A. Line Shapes

The absorption coefficient in $\mathrm{cm}^{-1}$ is given by

$$\alpha_j(\nu)=\{[(2\pi)^3/hcnV](\mathcal{E}_{\mathrm{eff}}/\mathcal{E})^2\nu\} \times\sum_{\mathbf{k}}\sum_{i} \mid M_i{}^j(\mathbf{k}) \mid^2\Delta(\nu-\nu_{\mathbf{k}}{}^e-\nu_{\mathbf{k}}{}^m). \tag{7.1}$$

Here $n$ is the refractive index, $(\mathcal{E}_{\mathrm{eff}}/\mathcal{E})^2$ is the effective-field correction, $\nu_{\mathbf{k}}{}^e$ and $\nu_{\mathbf{k}}{}^m$ are the wave numbers for the exciton and magnon, respectively, and $\mathbf{k}$ is summed over the first Brillouin zone. In the quantity $M_i{}^j(\mathbf{k})$ the superscript $j$ denotes the polarization of the light, and the subscript $i$ accounts for the various processes which can contribute. For example, $M_1$ refers to the

[55] M. Lax and J. J. Hopfield, Phys. Rev. **124**, 115 (1964).

process in which there is an exciton on sublattice 1, and a magnon on 2, while $M_2$ refers to an exciton on 2, and a magnon on 1. Since we shall consider the total absorption of the crystal due to intersublattice coupling, we include both $M_1{}^j(\mathbf{k})$ and $M_2{}^j(\mathbf{k})$. It is not difficult to show that there are only two distinct absorption coefficients: one for the electric vector parallel to the $z$ axis denoted by $\alpha_\pi(\nu)$, and one for the electric vector perpendicular to the $z$ axis denoted by $\alpha_\sigma(\nu)$. The absorption does not depend upon the direction in the $x$-$y$ plane because the $x$ and $y$ axes are equivalent when contributions from both sublattices are included.

Using Eq. (6.10) for the transition dipole moment, we find

$$\alpha_\pi(\nu)=C\sum_{\mathbf{k}}(|M_1{}^z|^2+|M_2{}^z|^2)\Delta(\nu-\nu_{\mathbf{k}}{}^e-\nu_{\mathbf{k}}{}^m)$$
$$=\Pi_X\sum_{\mathbf{k}}\sin^2(k_xa/2)\cos^2(k_ya/2)\cos^2(k_zc/2)\Delta(\nu-\nu_{\mathbf{k}}{}^e-\nu_{\mathbf{k}}{}^m) \tag{7.2}$$

and

$$\alpha_\sigma(\nu)=C\sum_{\mathbf{k}}[|M_1{}^\xi|^2+|M_2{}^\xi|^2]\Delta(\nu-\nu_{\mathbf{k}}{}^e-\nu_{\mathbf{k}}{}^m)$$
$$=\sum_{\mathbf{k}}\sin^2(k_zc/2)[\Pi_Z\cos^2(k_xa/2)\cos^2(k_ya/2)+\Pi_A\sin^2(k_xa/2)\sin^2(k_ya/2)]\Delta(\nu-\nu_{\mathbf{k}}{}^e-\nu_{\mathbf{k}}{}^m), \tag{7.3}$$

where the terms in the square bracket in Eq. (7.1) have been absorbed into the constants. Similar results have recently been obtained by Tanabe and Gondaira.[56]

We have labeled the three parameters as $\Pi_X$, $\Pi_Z$, and $\Pi_A$ because they multiply weighting factors which pick out the critical points $X$, $Z$, and $A$, respectively. For the most part, we treat them as phenomenological parameters. It is possible, however, to express them in terms of the pair matrix elements. For example, if we use Eq. (6.10), we have

$$\Pi_X=32C[|P_1{}^Z|^2+|P_2{}^Z|^2], \tag{7.4}$$

with similar expressions for $\Pi_Z$ and $\Pi_A$. Thus, it is possible to obtain experimental values for the pair matrix elements from the integrated sideband absorption coefficients.[52] Symmetry does not tell us the relative magnitudes and phases of $P_1{}^\xi$ and $P_2{}^\xi$. If we could obtain such information, we could determine the relative strengths of $\Pi_Z$ and $\Pi_A$ from the expressions of $\Pi_Z$ and $\Pi_A$ analogous to Eq. (7.4).

In evaluating Eqs. (7.2) and (7.3) we are faced with the problem of what to use for the exciton dispersion. We have the dispersion relation Eq. (4.13) but we do not know the parameters $K_1$ and $K_3$. With our present understanding of the exciton dispersion, the best we can hope to do is to obtain estimates of the parameters $K_1$ and $K_3$ which give the best agreement with the observed lines. We have calculated line shapes for several values of $K_1$ and $K_3$ by using a Monte Carlo technique, and we are led to the conclusion that it is not possible to obtain good agreement with both the observed profiles of $\pi1$ and $\sigma1$ for one set of parameters $K_1$ and $K_3$.

To indicate the problems one encounters, let us consider some possible parameters. We see from Eq. (4.13) that $K_1$ introduces dispersion in the $z$ direction and $K_3$ introduces dispersion in the $x$-$y$ plane. For an $X$ critical point only $K_3$ is important, for a $Z$ point only $K_1$ is important, and for the $A$ point both $K_1$ and $K_3$ are important. The observed profiles for lines $\pi1$, $\sigma1$, and $\sigma2$ are shown in Figs. 12(a) and 12(b). We can reproduce the peak position and shape of line $\sigma1$ rather well by using the known magnon dispersion and the exciton dispersion parameters $K_1=-1.3$ cm$^{-1}$, $K_3=0$. This moves the peak of $\sigma1$ to 57.4 cm$^{-1}$ as it should be and retains the sharpness of this line as shown in Fig. 12(c). These parameters, however, lead to a $\pi1$ line which is much too sharp and is at 50.4 cm$^{-1}$ rather than 41.7 cm$^{-1}$. To attempt to remedy this we try $K_3=4.3$ cm$^{-1}$ to move $\pi1$ to the correct position. As we see from Fig. 12(d) the characteristics of $\pi1$ are improved but $\sigma1$ has deteriorated. The relatively small value of 41.7 cm$^{-1}$ is the cause of this difficulty. A large dispersion parameter $K_3$ does not account for the observed properties. Moreover, it also seems unreasonable for $K_3$ to be considerably larger than $K_1$ since $K_1$ results from first-neighbor coupling and $K_3$ results from third-neighbor coupling. In the ground state, the third-neighbor exchange $J_3$ is negligible compared to $J_1$ and $J_2$.

One possibility for this difficulty may be the presence of phonons. Raman scattering [57] indicates that there is a low-lying optical branch with $B_{1g}$ character and 61 cm$^{-1}$ energy at $\mathbf{k}=0$. Its dispersion is not known. Thus it is conceivable that such phonons could influence these transitions.

We note that there are also difficulties in explaining the two-magnon line shapes even though the density of states is well known in that case. To account for the broadness of the two-magnon $\pi$ polarization line, Allen, Loudon, and Richards[10] have introduced a longer-

[56] Y. Tanabe and K. Gondaira, J. Phys. Soc. Japan **22**, 573 (1967).

[57] S. P. S. Porto, P. A. Fleury, and T. C. Damen, Phys. Rev. **154**, 522 (1967).

range interaction. This de-emphasizes the zone-boundary magnons and leads to the desired broadening. This may also be important for the exciton-magnon profiles.

The shape of line $\sigma 2$ can be reproduced rather well by using the exciton dispersion parameters $K_1=3.1$ cm$^{-1}$, $K_3=0$. The negative exciton dispersion pulls the peak down from 54.8 cm$^{-1}$ to 48.6 cm$^{-1}$. Line $\sigma 2$ does not have a sharp high-energy cutoff like $\sigma 1$ because, unlike the case for $\sigma 1$, the $Z$ and $A$ point exciton-magnon states do not have the greatest energy. It is significant, however, that the absorption does end rather abruptly at 54.8 cm$^{-1}$.

We see that the whole question of exciton-magnon line shapes is complicated, and not fully resolved. The strong polarization which results from symmetry is accounted for but the shapes which depend upon the exciton dispersion, the range of interaction, and possibly also upon other factors such as the phonons are not adequately accounted for.

### B. Stress Studies

The effect of uniaxial stress upon the sidebands in $MnF_2$ was first studied by Dietz, Misetich, and Guggenheim.[14] We have verified their results but shall not dwell upon this aspect of the problem except to point out how such studies are related to the present discussion.

For stress parallel to the $z$ axis ($S \parallel [001]$) lines $E1$, $\pi 1$, and $\sigma 1$ all shift by the same amount, and line $\sigma 2$ has the same behavior as $E2$. This provides strong evidence that $\sigma 1$ and $\pi 1$ are indeed sidebands of $E1$, and $\sigma 2$ is a sideband of $E2$. The stress studies do not indicate whether the sidebands are phonon or magnon sidebands; this information is provided by the shape, magnetic field, and temperature studies.

The lines do not split under a stress along the $z$ axis because the stress affects both sublattices in the same way. When the stress is applied perpendicular to the $z$ axis along the $\xi$ axis ($S \parallel [110]$) all of the lines split into two components (labeled $A$ and $B$ in Ref. 14). We remember that the ions on the two sublattices have environments differing by a 90° rotation about the $z$ axis. Thus, stress along the $\xi$ axis affects the two sublattices differently. For an ion on sublattice 1 (see Fig. 3) the stress tends to change the 78° bond angle of the four fluorine ions in the $\xi$-$z$ plane. This changes the orthorhombic crystal field which in turn changes the wave function $|e\rangle$. [The states $|g\rangle$ and $|m\rangle$, being orbital singlets, are insensitive to stress.] This produces an absorption with a complicated stress behavior. For an ion on sublattice 2 the stress is pushing directly upon a Mn-F bond. This does not cause a large perturbation upon the state $|e\rangle$ and the resulting transitions have a simple stress dependence.

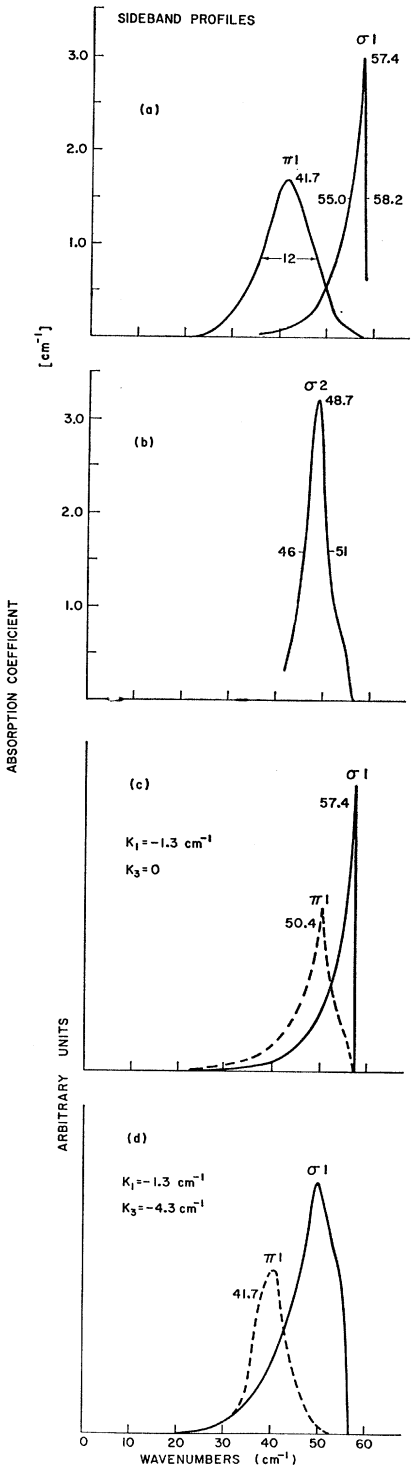


FIG. 12. The observed and calculated sideband profiles: (a) observed profiles for line $\pi 1$ and $\sigma 1$, (b) observed profile for line $\sigma 2$, (c) calculated profiles for lines $\pi 1$ and $\sigma 1$ using the exciton-dispersion parameters $K_1=1.3$ cm$^{-1}$ and $K_3=0$, (d) calculated profile for $\pi 1$ and $\sigma 1$ for the parameters $K_1=1.3$ cm$^{-1}$ and $K_3=4.3$ cm$^{-1}$.

Dietz *et al.* observe that $\sigma 1B$ and $\sigma 2B$ are seen when the electric field is perpendicular to the stress (along $\eta$) and $\sigma 1A$ and $\sigma 2A$ are seen for the electric field along the stress (along $\xi$). This indicates that the matrix elements $P_1^{\xi}$ and/or $P_2^{\xi}$ are much larger than $P_1^{\eta}$ and $P_2^{\eta}$.

The stress studies answer the question why line $E2$ does not have a sideband $\pi 2$. As stress is applied along the $\xi$ axis such a sideband appears. Dietz *et al.* have shown that the sideband strength is very sensitive to the structure of the excited-state wave function $|e\rangle$. In the unperturbed crystal, $\pi 2$ is simply too weak to be observed.

### C. Temperature Dependence

The temperature dependence of the energy separations $E1-\pi 1$, $E1-\sigma 1$, and $E2-\sigma 2$ provides a rather direct measure of spin-wave renormalization. Consider $\sigma 1$ for example. The peak of $\sigma 1$ corresponds to an exciton and a magnon with wave vectors at the $Z$ or $A$ points of the Brillouin zone. The peak wave number $\nu^{\sigma 1}(T)$ at a temperature $T$ is the sum of the exciton and magnon energies

$$\begin{aligned}\nu^{\sigma 1}(T) &= \nu_z^{e}(T)+\nu_z^{m}(T)\\ &= \nu_z^{e}(T)+R(T)\nu_z^{m},\end{aligned} \tag{7.5}$$

where $R(T)$ is the renormalization factor defined in Eq. (5.7). The energy $\nu^{\sigma 1}$ is measured and $\nu_z^m$ is known; however, $\nu_z^e(T)$ is not directly observable. To extract information about $R(T)$ we must relate the exciton energy at the $Z$ point to the observable energy of line $E1$ which is a $\mathbf{k}=0$ exciton. In other words, to gain information about the temperature dependence of the magnon dispersion, we must know something about the temperature dependence of the exciton dispersion.

We took the exciton dispersion to be independent of temperature in the 0–30°K region. We did this for two reasons. First, from the work of Gibbons[58] on the thermal expansion of $MnF_2$ and Dietz *et al.*[14] on the compression it appears that the parameters entering the exciton- and magnon-dispersion relations do not change with temperature in this region. Second, since the excitons have such large energies, these modes are unpopulated. Thus, there should not be any renormalization effects.

Thus, if we assume that the exciton dispersion is independent of temperature and define $(\sigma 1-E1)_T$ as the energy separation between $\sigma 1$ and $E1$ at temperature $T$, then from Eq. (7.5) we obtain

$$R(T)=1-[(\sigma 1-E1)_0-(\sigma 1-E1)_T]/\nu_z^m. \tag{7.6}$$

For lines $\sigma 1$ and $\sigma 2$ we use the $Z$, $A$-point magnon energy 54.8 cm$^{-1}$. For $\pi 1$ we use the $X$-point value 50.4 cm$^{-1}$. It is found that within experimental error the results for $\sigma 1$ and $\sigma 2$ are the same. These data are plotted as the solid circles in Fig. 7. The data for $\pi 1$ are plotted as $X$'s. The curves $R^1$, $R_x^2$, and $R_z^2$ are the theoretical renormalization factors obtained in Sec. V. C. For $R^1$ only the intersublattice exchange $J_2$ is considered and the result is independent of $\mathbf{k}$. When $J_1$, $J_2$, and $H_A$ are included the renormalization depends upon $\mathbf{k}$ and $R_x^2$ and $R_z^2$ are the results for the $X$, $M$ and $Z$, $A$, points, respectively. The curves marked AFMR and $M(T)$ are the experimental results for antiferromagnetic resonance[45] and sublattice magnetization,[59] respectively.

The optical studies and AFMR provide stringent tests of spin-wave theory. We see, for example, that $R^1$ which supposedly applies for all $\mathbf{k}$ does not agree with the AFMR experimental result (even when the error bars, which are as large as those for the sideband data, are considered). This is not too surprising, however, since $R^1$ neglects anisotropy which is a very important factor for $\mathbf{k}=0$ magnons. For the sidebands we compare the $\sigma 1$ and $\sigma 2$ data with $R^1$ and $R_z^2$ and the $\pi 1$ data with $R^1$ and $R_x^2$. It appears that the $\sigma$-polarization data is in somewhat better agreement with theory than the $\pi 1$ data. We see that the $\pi 1$ data agrees well with the AFMR result. It is not clear whether this has any significance. According to the theory, the $\pi 1$ results should be more similar to the $\sigma 1$, $\sigma 2$ results.

Again we see that difficulty arises with line $\pi 1$ and it is quite probable that the difficulties have a common origin. It is interesting to note that the observed temperature dependence of $\pi 1$ is well accounted for by renormalization theory if a maximum-magnon frequency of approximately 42 cm$^{-1}$ is assumed.

### D. Zeeman Studies

Experimentally, we find that a 10-kOe field parallel to the $z$ axis splits lines $E1$ and $E2$ by 1.7 cm$^{-1}$ while lines $\pi 1$, $\sigma 1$, and $\sigma 2$ show no apparent splitting or shifting. A field perpendicular to the $z$ axis has no effect upon any of these transitions.

The exciton and magnon Zeeman energies were obtained in Eqs. (4.12) and (5.4). It is clear that the Zeeman energy is the energy shift of a single-ion transition in a field and the energies can be obtained easily be referring to Fig. 5. We saw in Sec. III that the single-ion levels are unaffected by a field perpendicular to the $z$ axis. This explains the behavior in such a field. From the splitting of lines $E1$ and $E2$ we learn that $g'=2.11$ $(g=2.00)$.

For the sideband transitions we simply add the Zeeman energies. For example, for the final state $|E^1\mathbf{k};M^1-\mathbf{k}\rangle$ the energy shift is $\beta H_0(gS-g'(S-1)-g)$.

[58] D. F. Gibbons, Phys. Rev. **115**, 1194 (1959).

[59] V. Jaccarino and R. G. Shulman, Phys. Rev. **107**, 1196 (1957).

The shift for the final state $|E^1\mathbf{k}; M^2-\mathbf{k}\rangle$ is the negative of this; consequently the observed splitting is

$$\Delta_2=2\beta H_0(S-1)\,|\,g-g'\,|. \qquad (7.7)$$

If $g'=g$, the magnetic field will have no effect. In this case, the Zeeman energy of the magnon cancels that of the exciton. For the values $g'=2.11$ and $g=2.00$, the splitting should be 0.15 $cm^{-1}$ in a 10-kOe field. This is too small compared to the sideband linewidths to be observed optically. Russel, McClure, and Stout[13] have observed the Zeeman splitting for fields up to 170 kOe. For fields less than the critical field (approximately 90 kOe) the sidebands do not split. They observe, however, that line $\sigma 1$ does broaden in a way consistent with $g'=2.11$.

The Zeeman studies provide further evidence that the exciton and magnon are not on the same sublattice. The Zeeman energy of a state such as $|E^2\mathbf{k}; M^2-\mathbf{k}\rangle$ is approximately 1.7 $cm^{-1}$ in a 10-kOe field. If some of the sideband absorption strength results from intrasublattice coupling, the sideband would distort seriously in a magnetic field (even though the peak may not split since the weighting factors suppress all critical points for intrasublattice coupling). Such distortions are not observed in $MnF_2$.[51a]

We note that all single-ion transitions in $MnF_2$ or phonon sidebands of such transitions, should split in a $z$-directed magnetic field. Since all transitions are spin forbidden, the single-ion transitions must have a $\Delta M_s$ of at least 1. Barring highly unusual circumstances, such lines will split.

The pair transitions (i.e., sidebands) have the unique distinction that they are $\Delta M_s=0$ transitions (for intersublattice coupling). If the $g$ values of the excited states are reasonably near 2.00 such lines will exhibit no splitting. This provides a very convenient test to differentiate between sideband transitions and single-ion transitions. Unlike most other tests, this one does not require that the pure electronic transition be observed. For example, Eremenko and co-workers[7] have observed seven lines in the ${}^6A_{1g}\rightarrow{}^4T_{2g}({}^4D)$ region which do not split below the critical field. These lines are quite probably exciton-magnon transitions. McClure[17] has recently reported the results of a systematic Zeeman study of the optical spectrum of $MnF_2$. They find that *most* of the sharp electric dipole lines do not split below the critical field, thus, they identify these lines as exciton-magnon transitions.

## VIII. CONCLUSIONS

The concepts developed in this paper, and more thoroughly explored in the dissertation of Sell,[52] apply directly to all the sidebands in $MnF_2$, $FeF_2$, $CoF_2$, and other materials which have the magnetic space group $P4_2'/mnm'$. Using Loudon's[54] results we find that magnon sidebands in these materials should either be similar to those discussed here (excitons with $\Gamma_1^+$, $\Gamma_2^+$ symmetry) or should be similar to the two-magnon case (excitons with $\Gamma_3^+$, $\Gamma_4^+$ symmetry). The general framework which we have used should also be useful for describing sidebands in other materials, even with different symmetry. There were two central points in our discussion. First, the elementary excitations of pure materials are nonlocal propagating excitations which are characterized by a wave vector $\mathbf{k}$. This is a well-established concept but previously it was not recognized as an important factor in the optical spectra of magnetic insulators. The second and probably the most important point is that the elementary excitations, such as the excitons and magnons, can couple together to produce two-center excitations. It is not a mere coincidence that two-center excitations appear in magnetic materials. As we have seen, the Coulomb-exchange interaction provides the coupling between pairs of ions that leads to sidebands. This interaction is very similar to the exchange integral $J$ (in $J\mathbf{S}_1\cdot\mathbf{S}_2$) which causes magnetic ordering. Thus we expect some correlation between the existence of magnetic ordering and the presence of two-center excitations.

We have also emphasized that group theory is very helpful in identifying and characterizing sideband absorptions. At present, sidebands have only been observed in antiferromagnets. There appears to be no basic reason, however, why they should not appear in ferrimagnets and ferromagnets as well. The ferromagnetic case does present the unique feature that the exchange term cannot contribute (without spin-orbit coupling) since the $z$ component of spin must change in the transition. Sidebands in ferromagnets would probably result from the direct Coulomb interaction.

*Note added in proof.* Throughout our discussion of the exciton-magnon interaction, we have considered a completely aligned ground state for both the excitons and the magnons. Thus, the zero-point deviations of the magnons have been neglected and we have dealt with the $a_\mathbf{k}$ and $b_\mathbf{k}$ sublattice magnons rather than the coupled modes $\alpha_\mathbf{k}$ and $\beta_\mathbf{k}$ (see Sec. V.A.). Dietz *et al.*[60] have pointed out that the inclusion of zero-point deviations leads to two changes. First of all, the right-hand side of Eq. (6.10) for the transition moments due to intersublattice coupling are multiplied by $u_\mathbf{k}$. This leads to an almost negligible effect upon the calculated sideband profiles since these expressions pick out zone boundary critical points at which $u_\mathbf{k}=1$.

The second change is that the zero-point deviations introduce an additional intrasublattice coupling term which also conserves the total $z$ component of spin. This term is multiplied by $v_\mathbf{k}$ (which vanishes at the zone boundary). For the $z$ component, for example, the intrasublattice transition moment has the form

$$M^z(\mathbf{k})=2iv_\mathbf{k}[P_{100}{}^z\sin k_x a+P_{010}{}^z\sin k_y a],$$

where $P_{100}{}^z$ and $P_{010}{}^z$ are the coupling parameters for the third-nearest neighbors along the $x$ and $y$ axes, respectively. This term can lead to a line having the approximate position, shape, and Zeeman behavior of line $\pi 1$. However, this intrasublattice mechanism predicts that there should be a $\pi$-polarized sideband in the intrinsic emission with an integrated intensity approximately twenty times larger than the $E1$ emission line. Since no $\pi$-polarized sideband is observed in the intrinsic fluorescence,[60] we conclude that $\pi 1$ does not arise from this intrasublattice coupling mechanism.

## ACKNOWLEDGMENTS

We gratefully acknowledge the support and encouragement of Professor A. L. Schawlow, and the collaboration of Professor W. M. Yen during the early portions of this study. We also wish to thank Dr. Roger M. Macfarland and Dr. Robert Dietz for numerous helpful discussions, Professor R. Loudon for communicating his unpublished results, and Robert Feigelson for providing samples of $MnF_2$.

## APPENDIX: SYMMETRY OPERATIONS IN $MnF_2$

The complete magnetic space group $P4_2'/mnm'$ of $MnF_2$ consists of the operations listed below and their products with the subgroup of primitive translations $(E \mid \mathbf{t}_n)$ and $(\bar{E} \mid \mathbf{t}_n)$:

1. $(E \mid 0)$, the identity operator;
2. $(C_2{}^z \mid 0)$, a counterclockwise rotation about the $z$ axis through 180°;
3. $(I \mid 0)$, the inversion operator;
4. $(\sigma_h \mid 0) = (C_2{}^z \mid 0)(I \mid 0)$, reflection in the $x$-$y$ plane;
5. $(C_2{}^x \mid \boldsymbol{\tau})$, counterclockwise rotation about the $x$ axis through 180° followed by the translation $\boldsymbol{\tau}$;
6. $(C_2{}^y \mid \boldsymbol{\tau})$, counterclockwise rotation about the $y$ axis through 180° followed by the translation $\boldsymbol{\tau}$;
7. $(\sigma_{vx} \mid \boldsymbol{\tau}) = (C_2{}^x \mid \boldsymbol{\tau})(I \mid 0)$, reflection in the $y$-$z$ plane;
8. $(\sigma_{vy} \mid \boldsymbol{\tau}) = (C_2{}^y \mid \boldsymbol{\tau})(I \mid 0)$, reflection in the $x$-$z$ plane;
9. $(C_2{}^\xi K \mid 0)$, time reversal followed by a counterclockwise rotation through 180° about the $\xi$ axis;
10. $(C_2{}^\eta K \mid 0)$, time reversal followed by a counterclockwise rotation through 180° about the $\eta$ axis;
11. $(\sigma_{d\xi} K \mid 0) = (C_2{}^\xi K \mid 0)(I \mid 0)$, time reversal followed by reflection in the $\eta$-$z$ plane;
12. $(\sigma_{d\eta} K \mid 0) = (C_2{}^\eta K \mid 0)(I \mid 0)$, time reversal followed by reflection in the $\xi$-$z$ plane;
13. $(C_4{}^z K \mid \boldsymbol{\tau}$, time reversal followed by a 90° counterclockwise rotation about the $z$ axis followed by the translation $\boldsymbol{\tau}$;
14. $(C_4{}^{z-1} K \mid \boldsymbol{\tau})$, time reversal followed by a 90° clockwise rotation about the $z$ axis followed by the translation $\boldsymbol{\tau}$;
15. $(S_4{}^z K \mid \boldsymbol{\tau}) = (C_4{}^z T \mid \boldsymbol{\tau})(I \mid 0)$;
16. $(S_4{}^{z-1} K \mid \boldsymbol{\tau}) = (C_4{}^{z-1} T \mid \boldsymbol{\tau})(I \mid 0)$.

The coordinates $x$, $y$, $z$, $\xi$, $\eta$ are shown in Fig. 13 and $\boldsymbol{\tau} = a/2\hat{x} + a/2\hat{y} + c/2\hat{z}$.

We use the usual convention that the coordinate transformations $\mathbf{r}' = R\mathbf{r}$ given above correspond to transformations of functions $P_R\psi(\mathbf{r}) = \psi(R^{-1}\mathbf{r})$.

The point group of a crystal is the set of transformations obtained by setting all translations equal to zero in the space-group elements. The site group is the set of elements which leave one site invariant. For magnetic space groups we also differentiate between the unitary elements (no time reversal) and the antiunitary elements which include time reversal. The unitary elements form an invariant subgroup.

For this magnetic-space group, elements 9–16 are anti-unitary and 1–8 form the unitary subgroup $P_{nnm}$ or $D_{2h}{}^{12}$. Thus the unitary-point group is $D_{2h}$ and the unitary-site group is $C_{2h}$. The full point group is essentially $D_{4h}$, since the space group contains inversion as well as time reversal.

For $MnF_2$ in its paramagnetic state the space group is $P4_2/mnm$ or $D_{4h}{}^{14}$. It consists of the 16 elements given here with time reversal omitted. The site group is $D_{2h}$ and the point group is $D_{4h}$.

[60] R. E. Dietz, A. Misetich, H. J. Guggenheim, and A. E. Meixner (to be published).